Master's thesis

NTNU
Norwegian University of Science and Technology
Faculty of Engineering
Department of Energy and Process Engineering

Jakub Chrobak

Numerical and experimental study of vacuum freezing process

Master's thesis in Energy and Process Engineering
Supervisor: Associate professor Ignat Tolstorebrov
Co-supervisor: Dr Marek Rojczyk
August 2023

NTNU
Norwegian University of
Science and Technology

Jakub Chrobak

Numerical and experimental study of vacuum freezing process

Master's thesis in Energy and Process Engineering
Supervisor: Associate professor Ignat Tolstorebrov
Co-supervisor: Dr Marek Rojczyk
August 2023

Norwegian University of Science and Technology
Faculty of Engineering
Department of Energy and Process Engineering

NTNU
Norwegian University of
Science and Technology

ABSTRACT

The vacuum freezing is an alternative evaporative method of food freezing. The water content of the product evaporates due to the near-vacuum pressure in the chamber. Release of latent heat energy of the phase change causes the reduction of temperature and freezing of the product. The main objective of the thesis is to perform experimental investigation of the vacuum freezing process, and develop a not-present before 3-D numerical CFD model of vacuum freezing.

Temperature profiles depending on location have been measured to obtain a good understanding on internal heat resistance in the product. Experimental test have been performed on three different devices, each with different equipment and capabilities. A preliminary 3-D numerical model of vacuum freezing was developed, using enthalpy-based energy equation and approximations of thermal properties in function of temperature. The CFD model was validated with experimental results of vacuum freezing of pure water in RS sponge and vacuum freezing of potato slice.

Impact of cooling system, vacuum pump efficiency, and pressure in the chamber has been analysed and evaluated. Good agreement of temperature profiles was achieved in validation of potato experiments, and less satisfactory results have been acquired in the water RS sponge validation.

Based on results, achieving good agreement of temperature profiles is a challenging task in large bodies, due to the internal heat resistance. The development of the model could be a big step in advancement in simulating the vacuum freezing process, and further work towards the accuracy of the model should be done. The thermal properties and its change in function of pressure and temperature should be analysed to ensure the adaptation of the changing properties to increase the fidelity of the CFD model. Wider variety of food products should be experimentally investigated, to check the accuracy and agreement of the CFD model validation.

PREFACE

I would like to thank Prof. Ignat Tolstorebrov for valuable and truly helpful guidance during my stay in Trondheim. I was inspired to perform the investigation out of curiosity for the research subject. I would also like to thank Dr Michał Palacz and Prof. Jacek Smołka for the support during the challenging time of the work of this thesis. My thanks also go to Dr Michał Stebel, whose help with the food and freezing topic was invaluable. I also wish to thank Dr Michał Palacz, Prof. Jacek Smołka, Prof. Krzysztof Banasiak and Prof. Ignat Tolstorebrov for the opportunity to study in NTNU. Finally, I would like give my biggest thanks to my Julia, who supported me through highs and lows.

CONTENTS

LIST OF FIGURES

LIST OF TABLES

ABBREVIATIONS

Abbreviations:

CFD - computational fluid dynamics

EXP - experiment

GHG - greenhouse gas

NTNU - Norwegian University of Science and Technology

PLC - a programmable logic controller

SUT - Silesian University of Technology

STD - standard deviation

T1 - test 1

T2 - test 2

VC - vaccum cooling

VF - vacuum freezing

Roman symbols:

a - activity, –

c - specific heat, kJ/kg/K

cp - specific heat

D - diameter, m

h - specific enthalpy, kJ/kg

H - enthalpy, kJ

k - thermal conductivity, W/m/K

K - intrinsic permeability - m2

K_{evap} - evaporation constant, —

L - latent heat, kJ/kg

M - molar mass, kg/mol

p - pressure, Pa

r - radial coordinate, m

R_{evap} - evaporation rate, kg/m3/s

R - gas constant, kJ/K/kmol

S - source term, —

S - saturation in pores, —

T - temperature, degC

u - velocity, m/s

V - volume, m3

x - mass fraction , kg/kg

z - axial coordinate, m

Greek symbols:

δ - delta

μ - dynamic viscosity, Pa s

α - absolute permeability

ρ - density, kg/m3

ϕ - porosity

φ - volume fraction

Φ - general scalar, —

Γ - diffusion coefficient,

τ - time, s

σ - standard deviation, —

Subscripts:

a - air

ash - ashes

b - bound water

c - capillary

ch - chamber

eff - effective

f - frozen

g - gas

i - ith

I - first type of components

II - second type of components

ice - ice

if - initial freezing

in - inertial

$K-C$ - Kozeny-Carman

$Levy$ - Levy's thermal conductivity formula

$other$ - other components

p - pressure

pr - product

r - relative

ref - reference point

s - solid

sat - saturation temperature

unf - unfrozen

w - water

wo - moisture

v - vapour

CHAPTER

ONE

INTRODUCTION

1.1 Introduction

1.2 Green-house gases, environment, Green Deal

Greenhouse gas emissions (GHG emissions) are emission of gasses able to emit ultraviolet radiation such as carbon dioxide CO_2 methane CH_2 and nitrous oxide N_2O, that greatly contribute to unwanted climate change by not allowing part of the heat to escape to space [6]. It's a natural effect, but the intensity of GHG emissions and their concentration in atmosphere has been unnaturally high due to human activities [7]. In years 2010-2019 greenhouse emissions were at peak levels [8], and report by [9] shows that in 2022 GHG emissions were as high as equivalent of 41.3 Gt of CO_2. A sudden drop of increase trend was dictated by surprising outburst of sars-covid19, which reduced emissions, but with an unacceptable and impossible to maintain increase of cost. A European Green Deal (EGD) introduced in 2019 and approved in 2020 by The European Commission aims to reduce net greenhouse gas emissions by 55% by 2023 compared to 1990 levels, and to achieve zero net emission by 2050. According to Intergovernmental Panel on Climate Change (IPCC), in order to avoid increase of global warming above 1.5°C in upcoming decades, it is crucial to introduce net-zero policy to global emissions [10] throughout all of the high-emission sectors. Ensuring that strategy is a challenging but necessary task, that requires urgent reactions such as development of new technologies, and introducing them in sectors where greenhouse emission levels are specifically large. Such novel technologies must be focused at low-carbon emission and energy efficiency to maintain affordable cost. EGD is focused on few key sectors and aspects, with cold chain and cooling devices being two of them.

1.3 Modern cold chain

According to IPCC, 34% of greenhouse emissions are coming from energy supply sector, 22% from agriculture and 15% from transport [11]. A substantial share of the emissions are generated by a so called cold chain. Cold chain defines an in-order sequence of handling a food product from its harvesting to consumption while maintaining its temperature and humidity within appropriately low values, depending on type of product, such as vegetables, fruits, meats, dairy etc. Harvested goods often must be transported

between cities, countries or continents, meaning that it could take up to a few days from harvesting until the goods are placed into storage at distribution facilities such as supermarkets[12]. It's effectiveness is utmost important when taking account of food waste and loss, and failure in any part of the cold chain can cause the whole sequence in vain [13]. For this reason, securing reliability of each link individually greatly increases its effectiveness.

1.3.1 Food loss and food waste

According to various reports, globally, estimated 14% of produced food is lost between harvest and retail, and about 17% of food is lost in retail [14, 15, 16]. If combined, lost food could fed 1.26 billion people experiencing hunger, as stated by Food and Agriculture Organization of the United Nations (FAO) [17]. Food loss and waste results in not only the waste of food, but also all of the resources that were used to produce and transport this food, including energy, water, labour and land. Reports from The United Nations Food and Agriculture Organization indicate that post-harvest poor handling is one of the main reasons for food losses, particularly in developing countries [18]. For that reason developing and introducing new cooling and freezing technologies could vastly reduce food loss rates. Fruits and vegetables are especially prone to waste and perishment of their valuable properties such as vitamins, due to high moisture content.

1.3.2 Food safety

Safety of food is a utmost important matter, especially in developing countries. Unsafe food can be perceived as foods containing viruses, parasites, bacteria and toxic substances. Over the world, due to the unsafe food, each year 600 million people which is roughly 1 in 10 people, have symptoms after eating food, ranging from diarrhoea to even cancer [19]. Safety of the food is directly connected with the storage temperature and humidity, but also the rate at which product is being cooled, so ensuring a sufficiently fast cooling or freezing rate can increase food safety, by eliminating hazardous bacteria and microbial spores [20]. Lowering water contents of food reduces the growth of bacteria, which are a source of all kinds of diseases and decay of food products. For above reasons, choosing a cooling or freezing method capable of rapid cooling and freezing rate, while also reducing moisture of the product may greatly improve the food safety, thus reducing the number of people suffering from food contamination.

1.3.3 Food quality

Failure in maintaining low temperature during cold chain has an effect on factors such as taste, appearance, shape, color and texture. Properties such as texture, colour, pigments and taste are also dependent on humidity and moisture in the product [13]. Tian et al. [21] compared various cooling methods of broccoli, with the clear conclusion that the method of cooling has a worth noting impact on the quality of foods. Short cooling and freezing time contributes to the quality of stored foods [22], so the time of the process should be kept as low as possible while keeping the effectiveness of the process in the first place. Study done by He et al. [23] indicate, that the rate of pressure reduction has an effect on the quality and shelf-life of the goods. In the study, several pressure reduction rates were used during the process, with a conclusion that a moderate reduction rate of

313 Pa/second from 10000 Pa to 600 Pa was the most beneficial in terms of quality of the product. For the above reasons, a compromise between fast process and a moderate pressure reduction rate should be found to find the optimal operation parameters.

1.4 Cooling and freezing methods

Before food can be transported in low-temperature environment to its distributors, it must be properly cooled or frozen within short and acceptable time in order to maintain satisfactory, and most importantly required safety and quality, while also to extend shelf life of the product. Lowering temperature of goods reduces rate of disease and bacteria development, helps maintaining nutrition and minimises cooling capacity during later transportation [24]. Studies indicate that ensuring effectiveness of initial cooling and freezing may be the most important link in cold chain. Most popular freezing methods are:

Air freezing

Air freezing is a very commonly used method of freezing in which the still or moving cold air, usually between -35 °C to -52 °C [25] is treated as a freezing agent. Food is stored in shelves in which the cold air is present, and therefore its temperature is reduced. This method is characterised by very low cost of maintenance and constant coolant temperature. While it is the cheapest method, its also the slowest due to the low heat transfer coefficient of air. There are various types of air freezers, such as sharp freezer, tunnel freezer, batch freezer, belt freezer, which are constructed and operate different, the premise is the same. Usually, the products froze by this method are meats, fish, fruits, vegetables or dough. [25] The biggest advantage of this method is the simplicity and low cost, but with the cost of low heat transfer rate and uneven air distribution [26].

Fluidized bed freezing

In that method, the product is placed on a bed with perforated surface, from below which the high-velocity cold air is blowing, which results in the floating of the product. Because of that, the product is surrounded by the cold air and the heat thermal coefficient is quite high. Because of the individual quick freezing character of this method, it is mostly used for a small foods such as small vegetables, fruits, diced meat [27]. Compared to the air freezing method, the operational and capital cost is higher, but since the foods are in greater contact with the air, the freezing is quicker and more uniform, but foods that can be frozen are limited due to the size requirement.

Contact freezing

Contact freezing is a method where the frozen good is directly or indirectly in contact with the surrounding freezing medium. Because of that, the heat thermal coefficient is very high, therefore the process is viewed as an efficient. Contact freezing when compared to the traditional air freezing helps preserving the quality of the product and the time of the process is slower, but may cause some unfavourable changes in food texture and properties.

Immersion freezing

Basis of the immersion freezing is to place the product in a tank, and immerse it in the cooling medium. As in the above methods, because the product is surrounded by the freezing medium, the heat thermal coefficient is high. Its important to use a neutral medium, which won't affect the taste, smell, composition or color of the immersed product. The operational time of this process is quicker [28], but the efficiency of the coolants usage is quite low [29].

1.5 Vacuum freezing

Vacuum freezing is an alternative method of rapid food freezing using phase-transition, in which the water content of food products is evaporated by decreasing pressure in the food chamber up to a near vacuum. Phase change from liquid to gaseous state requires high amount of energy called latent heat, and with the product being the only body inside the chamber, the energy required for phase change of water is taken from the product in form of sensible heat, resulting rapid cooling effect. As chamber pressure is reduced, so is water saturation temperature which is directly related to the temperature of evaporation. When the water pressure and temperature drops to 611.657 Pa and 0 °C respectively, it reaches the so-called triple point, below which the phase change occurs in form of sublimation, so from solid state (ice) to gaseous state (vapour), omitting the liquid state which should not be present in the system below these parameters. According to various studies [13, 20, 21, 30], vacuum cooling and freezing method improves the shelf life of certain foods, such as fruits and vegetables, increases the food safety and helps keep the nutrition, texture, and overall quality of the product. When compared to standard freezing methods, vacuum freezing method reduces the time required to reach desireably low temperature while improving temperature distribution, and depending on the product, can have lower running cost at the expense of high capital investment [21].

1.6 Research gap

Numerical simulations of vacuum cooling process are mentioned in papers [31, 32, 33, 34, 35, 36, 37] however deep research regarding simulations of vacuum freezing process is almost non-existent, with a few exceptions analysing simple model [38, 39]. Better understanding of vacuum freezing is even more important, as its a crucial part of widely used freeze-drying. Freeze drying model is much more complicated, due to mutual existence of 3 phases, its phase change interface, supercooling effect and introduction of additional coefficients related with freezing.

1.7 Motivation

The current state of global warming and the hunger in the developing countries is an issue that needs to be addressed as soon as possible. Making even a small step towards the decrease of number of people that go to sleep with the sense of hunger is a crucial task in author's eyes. The improvement of the cold chain and pre-cooling and pre-freezing stage could realistically reduce the GHG emissions, food waste and food loss. For the above reasons, the investigation of alternative cooling and freezing methods should be performed.

To the best knowledge of the author, an in-depth 3-D CFD numerical model of vacuum freezing has not been developed yet.

CHAPTER
TWO

THEORETIC ASPECTS OF VACUUM FREEZING

2.1 Vacuum freezing process

If considering vacuum freezing of a small water sample, it can be assumed that its properties and temperature is the same at any point of a body. In such case, when pressure around the product is reduced below saturation pressure corresponding to initial temperature of water, it will start to evaporate and in consequence, as mentioned in Section 1.5, lower its temperature due to the latent heat of evaporation. With pressure still being reduced, temperature of water sample will drop to initial freezing point of 0 °C, but there will not be any freezing. The phenomena when a liquid's temperature is being lowered below its freezing point without freezing is called supercooling. The temperature will continue to drop until nucleation and phase change occurs. Nucleation is a spontaneous process that takes place within a known range of temperature, but the exact moment is random. The nucleation process is influenced greatly by the purity of frozen media. In 100% pure water nucleation occurs approximately in -35 °C, whereas introducing even not noticeable by an eye impurities to the system can increase the temperature of nucleation up to -5 °C and warmer [40, 41, 42]. Energy released due to the latent heat of phase change causes the increase of local temperature up to a freezing point, and the temperature will not drop for duration of time during which liquid is freezing. When all of the liquid water is frozen, temperature will start to drop again, without any further obstacles.

With the overall premise process explained, it is important to take into the account a body characterized with mass and volume, which causes the occurrence temperature profiles across the product. In such case, the temperature of the surface will be firstly reduced, and will be the coldest part of the body through the process, due to the evaporation being the most intense there. This is caused by the permeability of the product, which causes the pressure to be reduced at slower rate in inner parts of the body, thus the driving force of the cooling and freezing - difference between saturation and partial pressure is the highest at the outer part of the body. Temperature will be reduced the least in the core of the body, and with very low or non evaporation occurring in the core, heat transfer from the outer parts of the product is the main source of temperature drop and therefore is a crucial factor of vacuum freezing process when dealing with products of high volume. As soon as surface temperature reaches initial freezing point, the water in the surface will undergo supercooling, which will be interrupted by nucleation and phase change, just to return to further freezing. Created ice at the surface will now be

moving inwards into the core as the freezing front, at which phase change occurs. The moment when freezing front reaches the core of the product is the moment when whole product is frozen [43]. With the exception of certain foods such as meat, where the goal of the process is to reach a certain temperature in the surface, for this case, the end of the process should be defined by the core of the product reaching desirable temperature.

2.2 Time of vacuum freezing

2.2.1 Product

Type of product undergoing vacuum freezing has crucial influence on the process, making some foods ineligible for the process, while certain foods benefit from the this type of freezing heavily. As vacuum freezing is type of evaporative freezing, foods ratio of surface to volume is exceptionally important. High ratio of product surface to its volume improves the rate of evaporation, since water vapour can leave the product only through its surface, so increasing evaporation area directly increases the amount of water that can evaporate in the time period. For this reason vacuum freezing product such as whole fruit and vegetable will take much more time than if the fruit would be cut into slices and placed individually, therefor increasing the surface while the volume of the load remains the same. The influence of the product on the time of vacuum freezing process, is almost purely dependent on the initial water content, surface to volume ratio. In case of large bodies, reducing temperature will take much longer, because temperature drop is dependent on ratio of mass evaporated to initial mass of the moisture in the product, so the amount of water that needs to be evaporated from much heavier product is significantly higher. In such cases the usually very slow internal heat transfer plays a crucial role in reducing the temperature of the core, since almost no water is evaporating from the inside of the product.

2.2.2 Process parameters

Time required for the temperature drop of a specific product during vacuum freezing process is for the most part dependant on the pressure inside the vacuum chamber, as it is the driving force behind the evaporation rate which causes loss of heat. Therefore, the main role of equipment used in vacuum freezing is either to reduce or keep the pressure in the system as low as desired and possible.

2.2.2.1 Freezing system

Freezing system consists of an evaporator, refrigerant and cooler. Main function of the evaporator is to protect the vacuum pump which sucks the vapour (and air) from the chamber. If cold vapour will get into the vacuum pump it would condensate and coalesce with the pump oil and significantly reduce it's vacuum capacity. Inside the evaporator there is a coil in which the cold refrigerant flows, and causes the temperature of the coil's outer surface to be similar to the temperature of the refrigerant. The evaporated water vapour flows from the chamber to the evaporator, and due to the difference in temperature between the water vapour and the coil temperature it condenses on the coil's surface. The partial pressure of the now condensed ice is equal to saturation pressure in the corresponding temperature of the coil. So the lower the temperature of the coil,

the lower the condensed ice partial pressure, and in consequence the lower the resulting pressure in the system. Cooler is constantly keeping the refrigerant in sufficiently low temperature.

2.2.2.2 Vacuum pump

The vacuum pump for vacuum freezing process should be well-fitted to the rest of the equipment. Vacuum pump is responsible for reducing the pressure in the vacuum chamber, by creating a low pressure at its inlet, thus making gases rush from inside the chamber to the vacuum pump. By removing gases from the vacuum chamber, the pressure is reduced. Pumping speed of vacuum pump measures the volumetric flow rate across a plane at a specific pressure. The pumping speed is a function of the pressure at the plane where the gas is being pumped out of. The lower the pressure in the chamber, the lower the density of pumped gas, thus much more volume needs to be pumped out to reduce the same mass of vapour as in atmospheric pressure.

2.3 Thermal properties of food products

First step of creating a thorough simulation of vacuum freezing process is to as accurately as possible approximate the properties of food product. Determination of initial properties of a certain food product can be done through various experimental methods. Properties of foods vary greatly from meats to fruits, vegetables, dairy etc., but also between different types of vegetables and even the same exact product from the same batch. For example, thermal properties of one potato can be very much different from another potato. Choosing products from the same batch, in similar sizes and same temperature, humidity etc. can possibly reduce the differences between two samples, but its impossible to determine without testing it experimentally. During vacuum freezing process, food go through changes in temperature and phase, which results in change of thermal and physical properties such as specific heat, enthalpy, thermal conductivity and density. During a very short range of temperature within which food undergoes phase change in form of freezing, specific heat jumps very intensively, increasing the amount of heat that is required to increase its temperature. The precision of specific heat to temperature relation is utmost important in freezing calculations, because the specific heat affects the thermal conductivity of the material, which is crucial in simulating the temperature distribution within the product during the freezing calculations. For that reason, many theoretical methods and empirical equations based on experimental data and have been made to approximate the food properties, taking into the account the most influential properties, such as water content, composition in form of soluble and insoluble substances such as acids, sugars, fats, starch etc., temperature, type, porosity.

2.3.1 Chen's enthalpy approach

C.S. Chen [44] proposed a temperature-enthalpy correlation to describe the enthalpy and apparent specific heat of foods undergoing the process of freezing. Approach proposed by the author creates the correlation of temperature to enthalpy based on calorimetric investigations. His approach also takes into the account the latent heat of freezing when calculating the apparent specific heat, thus introduction of additional heat source term responsible for simulating the release of energy of latent heat becomes unnecessary. A

mathematical equation is proposed, with constants depending on composition and moisture content of certain food, which makes the approach eligible for various food products. Specific heat of a food product is calculated based on the fraction of solids, namely sum of proteins, fats, carbohydrates, fibers and organic compounds, which when summed with water content, add up to 100%. A distinction in mathematical equation for specific heat is made with respect to temperature of freezing point, because the as the freezing process begins, latent heat of freezing must be included. During phase change, depending on moisture content, specific heat indirectly increases tens to hundreds of times, meaning that it requires very high amount of energy to increase its temperature by even 0.1 °C. This is due to the energy required for solidification which is equal to 333.6 kJ/kg, while specific heat of water is approximately 4.2 kJ/kg/K. This means, that energy required for phase change of 1kg of water is equal to energy required to cool 1kg of water by almost 80 °C, or cool down 80 kg of water by 1 °C. Therefore, separate apparent specific heat above Eq.(2.1) and below Eq.(2.2) freezing point is calculated:

$$c_{unf} = 4.19 - 2.3x_s - 0.628x_s^3 \tag{2.1}$$

$$c_f = 1.55 + 1.26x_s - \frac{x_{wo} - x_b L T_{if}}{T^2} \tag{2.2}$$

where x_s is is the mass fraction of solid components, x_{wo} is the mass fraction of moisture, L is the latent heat of fusion of water $[kJkg^{-1}]$, T_{if} is the temperature of initial freezing of food product $[°C]$ and T is the temperature of food product $[°C]$.

The apparent specific heat can be defined as change of enthalpy divided by change of temperature:

$$c = \left(\frac{\partial H_f}{\partial T}\right)_p \tag{2.3}$$

where H_f denotes the enthalpy below initial freezing point $[kJ/kg]$. Using the specific heat equations Eq.(2.1) Eq.(2.2) and integration of specific heat-enthalpy relation Eq.(2.3), a formulation for enthalpy corresponding to temperature above Eq.(2.6) and below Eq.(2.4) freezing point is given:

$$H_f = h_{if}\left(T - T_{if}\right)\left(4.19 - 2.30x_s - 0.628x_s^3\right) \tag{2.4}$$

$$h_{if} = \left(T_{if} - T_{ref}\right)\left(1.55 + 1.26x_s - \frac{\left(x_{wo} - x_b\right) L T_{if}}{T_{ref} T_{if}}\right) \tag{2.5}$$

$$H_{unf} = \left(T - T_{ref}\right)\left(1.55 + 1.26x_s - \frac{\left(x_{wo} - x_b\right) L T_{if}}{T_{ref} T}\right) \tag{2.6}$$

where T_{ref} is temperature in reference point $[-40°C]$, and h_{if} is specific enthalpy of the food product at the initial freezing point $[kJkg^{-1}]$.

2.3.2 Thermal conductivity

Thermal conductivity is a relevant and a very important property that needs to be heavily considered for freezing calculations. It denotes the rate at which temperature is heat is transported within the product. High thermal conductivity favors high freezing

(a) Apparent specific heat in function of temperature (b) Apparent specific heat in function of enthalpy

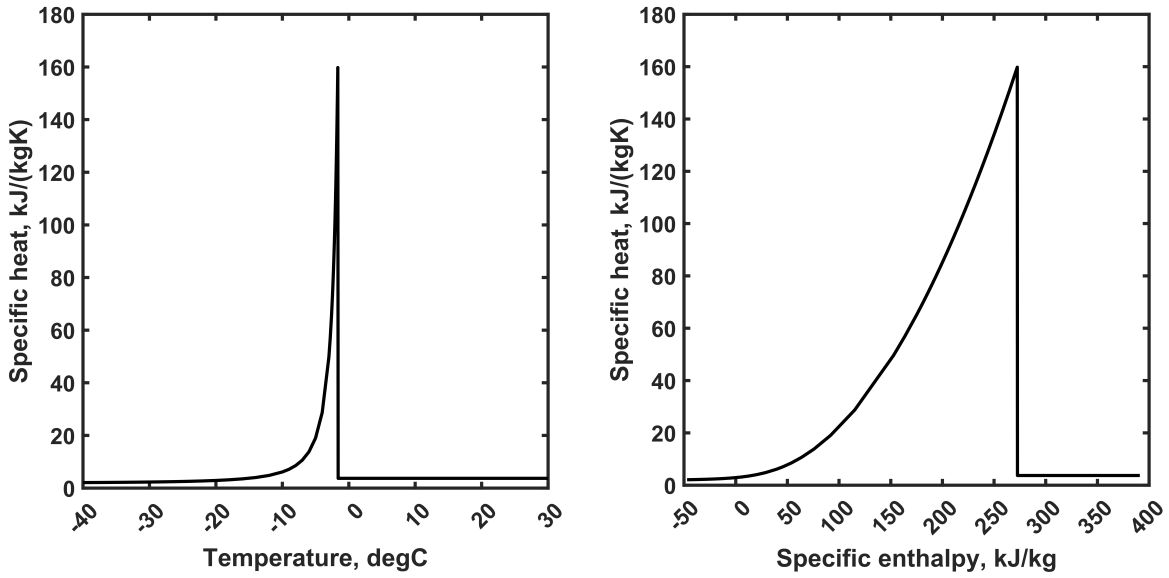

Figure 2.3.1: The apparent specific heat in function of temperature and enthalpy

uniformity, since difference in temperatures within the product can be quickly reduced. Thermal conductivity of food products is a function of temperature with a large change around the freezing point [43]. Several mathematical models were developed based on the application such as non porous unfrozen foods, frozen porous foods etc. For porous and especially, frozen foods, thermal conductivity changes drastically the freezing point due to the appearance of ice, because the thermal conductivity of ice is significantly higher that liquid water or any other components which are present in foods [45]. Levy [46] proposed a thermal conductivity model that takes into the account the properties of ice, and calculates the effective thermal conductivity based on the volume fractions of ice and other components, such as liquid water, proteins, fats etc:

$$k_{levy} = k_{ice}\frac{2k_{ice} + k_I - 2\big(k_{ice} - k_I\big)F}{2k_{ice} + k_I + \big(k_{ice} - k_I\big)F} \tag{2.7}$$

Where k_{ice} is the thermal conductivity of ice and k_I is the thermal conductivity of the continuous phase, so liquid water, proteins, fats, etc. F and G are functions describing the composition and thermal conductivity, where function F is:

$$F = \frac{\frac{2}{G} - 1 + 2\big(1 - x_{ice}\big) - \sqrt{\big(\frac{2}{G} - 1 + 2\big(1 - x_{ice}\big)\big)^2 - 8\frac{\big(1-x_{ice}\big)}{G}}}{2} \tag{2.8}$$

and function G is represented by:

$$G = \frac{\big(k_{ice} - k_I\big)^2}{\big(k_{ice} + k_I\big)^2 + \frac{k_{ice}k_I}{2}} \tag{2.9}$$

2.3.3 Initial freezing point

Initial freezing point can be described in a couple of ways, but essentially, initial freezing point is the highest temperature at which freezing process can start. In another words, the highest temperature at which any ice crystal can be present. From vacuum freezing point of view, it defines the beginning of the freezing process, or temperature at which nucleation can occur. Initial freezing point of food products is dependent on its composition of properties such as water content (moisture), but also proteins, fats, carbohydrates, organic fraction and fibers. Initial freezing point of product containing 100% pure water is equal to 0 °C, but presence of properties mentioned above, such as proteins and fats reduce the initial freezing point based on their fraction [42].

2.3.4 Ice content

As was already established, formation of ice is a gradual process that takes an effect after temperature drops below initial freezing point. Estimation of ice content in food freezing calculations is crucial due to the difference in thermal and physical properties between ice and liquid water. Ice fraction as a variable is used in many approximations, for example the previously mentioned Eq. 2.7 used to calculate thermal conductivity of food. [44] described a variety of methods to calculate ice fraction of a material, which can be based on composition, or initial freezing point. In case of simulating freezing of a specific food containing a significant amount of fats, proteins, carbs etc., a mathematical model should be chosen based on agreement of a certain model with experimental data of specific food. An equation for estimating ice fraction of frozen food was given by Tchiegeov [47]:

$$\varphi_{ice} = \big(\varphi_w - \varphi_b\big)\big(1 - \frac{T_{if}}{T}\big) \tag{2.10}$$

Where φ is the volume fraction of φ_{ice} ice, φ_w water and φ_b bound water, T_{if} is the temperature of initial freezing point and T is current local temperature.

2.3.5 Porosity and permeability

The material of porous foods can be described as a unsaturated porous media. The pores within a product are only partially filled with moisture, and rest of the pore volume is filled with air. Permeability of the material or product measures the ability of a liquid or a gas to pass through the material. In case of vacuum freezing porous foods it defines the ability of passage of fluid through the pores. It's dependent on pressure and composition of flowing fluids, since the permeability is not only affected by the material, but also the media which is passing the material. Various experimental studies have been carried out to assess the permeability of certain foods. Feng [48] managed to validate a Kozeny-Carman equation [49] that calculates the permeability based on porosity and a fiber or grain diameter with experimental data of apple tissues:

$$K_{K-C} = \frac{D^2}{180}\frac{\phi^3}{\big(1-\phi\big)^2} \tag{2.11}$$

where D is the diameter of the volume equivalent spherical particle and ϕ is the porosity of the material.

CHAPTER

THREE

EXPERIMENTAL AND NUMERICAL ANALYSIS OF VACUUM FREEZING

3.1 Experimental and numerical analysis of vacuum freezing

3.1.1 Water RS sponge sample analysis

To analyse the vacuum freezing process, experimental and numerical analysis of pure water in a RS sponge was performed. The analysis of pure water can ensure the accuracy of well documented thermal and physical properties of sample. If the experiment would analyse the vacuum freezing of free water, the boiling would cause extreme spillage and increase of evaporation surface, therefore reducing the accuracy of input parameters in the CFD validation model, or even causing the model to be completely inaccurate. For this reason, the RS sponge is behaving as a vessel, in which the water is trapped, just as in food sample.

3.1.2 Food sample analysis

To prove the striking similarity in experimental process of vacuum freezing of RS sponge, visible in Fig. 3.1.1 and its parameters show in 3.3.1, food, and moreover the applicability of the CFD model to simulating vacuum freezing of food products, the experimental and numerical analysis of a potato slice was conducted. Ultimately, the aim of the numerical model is to create a straight-forward model that can simulate the vacuum freezing process of various foods with a satisfactory accuracy of temperature and mass reduction in given time of the process. For that reason, experimental vacuum freezing of potatoes was performed and validated with created CFD model.

3.2 Water RS sponge experimental analysis

3.2.1 µWaveVac0250 apparatus

The µWaveVac0250 apparatus consists of the vacuum chamber, vacuum pumps, microwave system, cooling unit, condenser and PLC [50]. µWaveVac0250 is a microwave freeze dryer used for freeze drying loads up to 50 liters using vacuum and microwaves. The

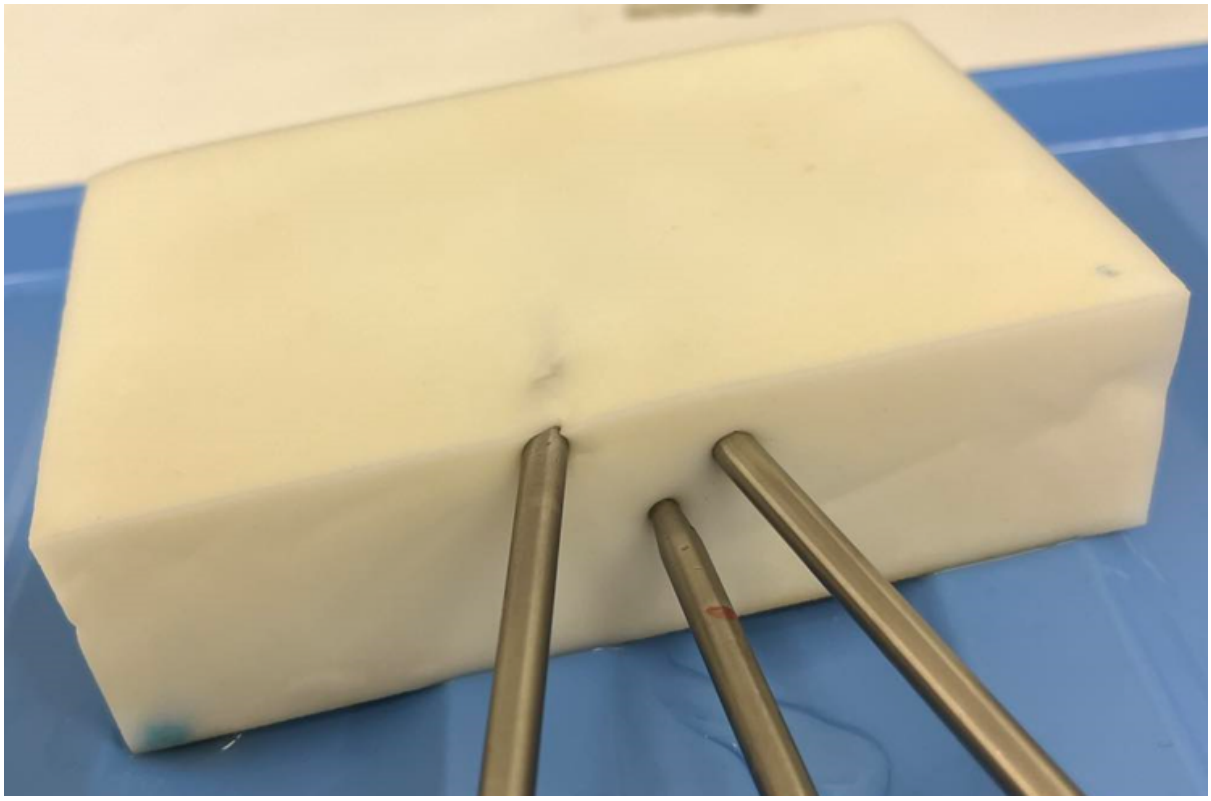

Figure 3.1.1: RS sponge filled with pure water, before vacuum freezing process

vacuum chamber has a large capacity of 50 liters, and can operate with a turntable, open and closed rotating drum, and without any internal movement. The microwave system as well as the use of a rotary functions are intended for microwave-induced freeze-drying. Two vacuum pumps are responsible for reducing the pressure in the system, Pfeiffer Okta 500, with very high pumping speed in near-vacuum pressure shown in Fig. .0.1, and Pfeiffer Duo 65, with its characteristic shown in Fig. .0.2. This plant is equipped with a Huber Unistat 905 temperature control system, capable of keeping the temperature of a refrigerant as low as -90 °C [51], and gives precise control of its temperature. The condenser and coil cooling capacity exceed the amount of vapour that can be evaporated from a sample used in experimental tests. Built-in PLC allows for measurements of pressure recorded during the process. In addition to the pressure readings, µWaveVac0250 apparatus allows for measurements of food sample mass reduction related to water content evaporation, so tests done in that equipment allow for observing mass loss caused by evaporation and sublimation, in a function of time. The pressure in the vacuum chamber can be controlled by a WaveCAT software, as well as manual setting directly on the machine. Due to a different purpose of this equipment, setting pressure in the chamber below 1000 Pa results in a pressure with wide range of inaccuracy, between 700 Pa and 100 Pa. For this reason, the tests were done in a system where vacuum pumps are constantly working, but to reduce the outcome pressure in the chamber, the temperature of the cooling system was set to -10 °C. Such operation increases the partial pressure of the evaporated water vapour that sediments on the evaporator, resulting in increased pressure in vacuum chamber. This device is characterised by high pumping speed, large evaporator/condenser and cooling system capable to reach -60 °C.

3.2.2 LyoCube Martin Christ apparatus

The LyoCube 4-8 LSCplus Martin Christ device is a laboratory freeze-dryer equipped with vacuum chamber, 5 shelves, condenser, vacuum pump and a PLC. Vacuum chamber is designed for a small scale laboratory tests, with chamber dimensions of 39 x 43 x 37 cm [52]. Inside the chamber there is a rig dedicated to placing 5 shelves, on top of which the sample can be placed. Temperature of each shelf can be controlled within a range of -35 °C to 60 °C. Condenser maximum ice load is equal to 4 kg, and its temperature can be reduced up to -85 °C. Vacuum pump connected to the chamber is a Edwards 12 RV12 Rotary vacuum pump [53], and its characteristic is shown in Fig .0.3. During the time of experimental tests, shelf temperature control, as well as condenser were not used. Thus, pressure reduction rate in this device will be smaller, and the chamber pressure at which the reduction rate will greatly decelerate will be higher when compared with the µWaveVac0250 apparatus, due to much lower pumping speed, and also the lack of condenser and cooling unit. The PLC used in this device provides the information only about pressure in the chamber, so evaporated and sublimated mass can be checked only after the process, giving information about lost mass during the whole process.

As it was briefly described above, the discussed systems were designed for completely different loads. Hence, the equipment of the vacuum freezing process could be studied in systems of completely different scales.

3.2.3 Sample

Food composition and structure is a complicated matter which varies even within the same batch of fruit and vegetable, so describing it precisely without much-needed measurements is a challenging task. Mathematical models simulating physical phenomena should contain as few uncertainties as possible to eliminate the possibility of wrong input properties when analysing possible inaccuracies, and in later stages achieve high agreement with experimental data. For that reason, food sample was replaced by an RS PRO ESD Sponge filled with tap water, that can be seen in Fig. 3.2.1. Consequently, the thermal properties and structure of the water RS sponge sample were defined with significantly higher accuracy comparing to the real food sample.

3.2.3.1 Preparation

Three holes visible in Fig. 3.2.1 were made in RS sponge, each in different distance from the surface, to investigate temperature in different parts of the sample. Before each run, the sponge was weighted as dry, and immersed overnight in a bucket of fresh tap water and placed into the fridge and cooled down to 5 °C. Water was changed each time to ensure no change in the composition of the fluid. Since ambient temperature in the laboratory was measured about 22 °C, during the time of transporting the sample from the fridge to the apparatus, the sample was put in insulating styrofoam box which was being held in the same temperature as the sample. Before running the test, sample was weighted directly before installing the temperature sensors in insulated sponge holes, and then placed into the vacuum freezer to undergo the process. The thermometers were put in slightly angled, so the tip of the sensor is as close as possible in the middle of height, width and length of the sponge. The angle and exact position of thermometers can be seen in Fig. 3.2.1. The thermometer at the surface of the product could not have been placed closer to the surface, because during the vacuum freezing, the sponge would rip at

the location due to the thin layer between probe and surface, causing the thermometer to show mixed temperature of sponge and ambient air.

Figure 3.2.1: RS sponge after the vacuum freezing, with visible locations of measurements

3.2.3.2 Measurements

Temperature was measured by three testo915i Wireless Digital Thermometer with immersion/penetration probe in the core, close to the surface and in between those 2 points which will be further called middle. Such setup allows not only for studying freezing time in different location of samples undergoing vacuum freezing process, but also provides information about the temperature profiles. The exact location of probes, as well as the stand at which the sponge stood during the vacuum freezing can be seen in Fig. 3.2.2

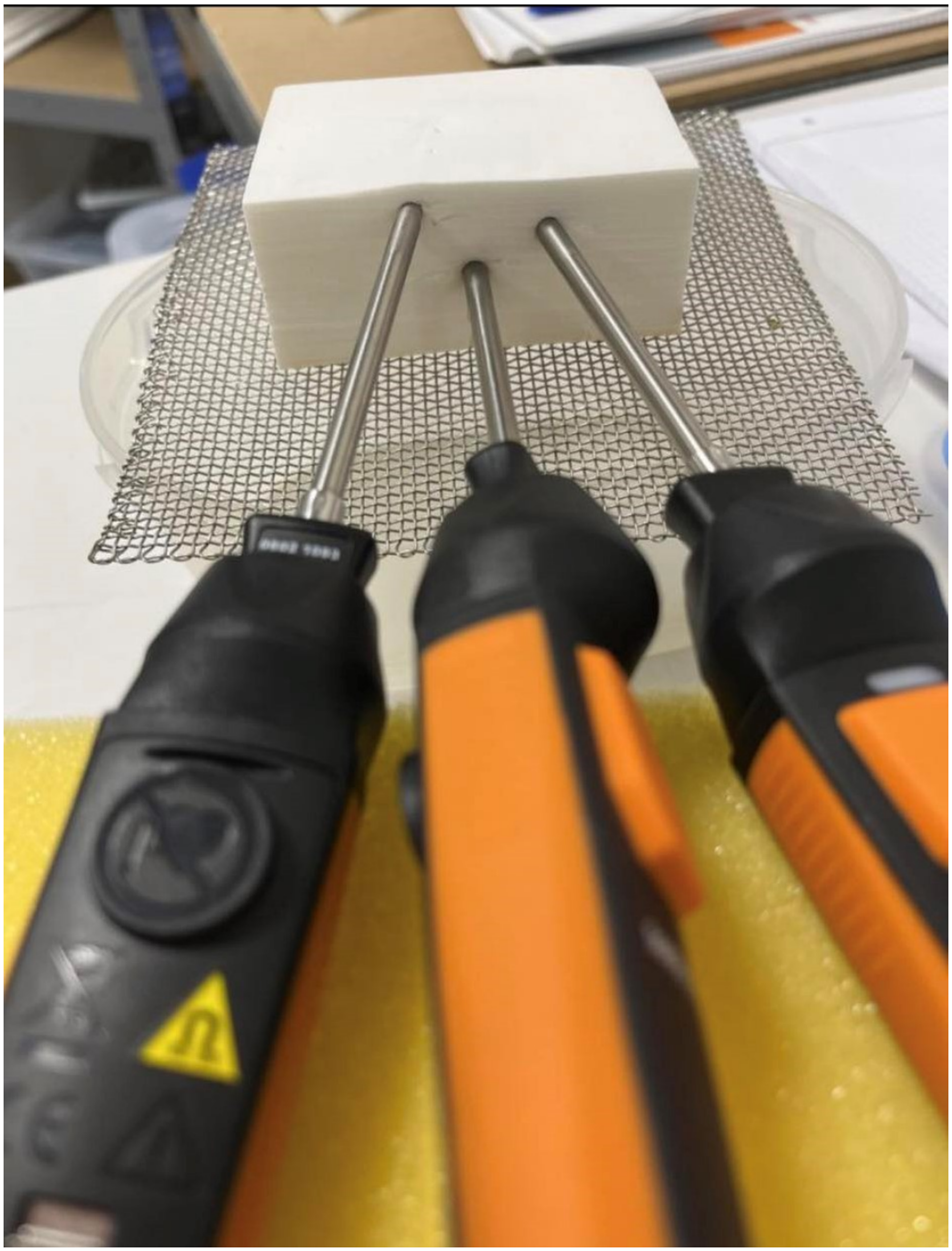

Figure 3.2.2: RS sponge with temperature senors before the vacuum freezing process

3.2.3.3 Pre-processing

In contrary to food products such as fruits and vegetables, the surface of RS Sponge does not prevent water from spilling out during depressurisation, which means that during the process of lowering pressure inside the chamber, water will start to spill out of the sponge. The reason for this phenomena is a high level of air saturation in water, which can be conveniently reduced by the process of vacuum cooling. Reducing the pressure of the water-filled RS Sponge will cause the water and air saturated in it to evacuate and spill out of the sponge. Because of that, RS Sponge is placed on metal mesh over a plastic

box, so the water is spilt directly into the box, preventing the insides of the chamber from a mess. The sample prepared in this way was subjected to a vacuum cooling process, which stopped before any point of the product temperature dropped below 0.5 °C so that the structure of the sponge was not alternated by the appearance of ice. As soon as the temperature have reached the desired level, the vacuum is broken and the sponge is set to rest in -5 °C environment until a temperature equilibrium is met in the sponge.

3.2.3.4 Vacuum freezing

Vacuum freezing begins when the vacuum pumps starts reducing pressure, and ends when a desirable temperature in the core of the product is reached.

3.3 Food experimental analysis

3.3.1 VacPCM apparatus

The VacPCM apparatus that can be seen in Fig. 3.3.1, is an experimental test rig designed specifically for experimental analysis of vacuum freezing process, and it consists of a vacuum chamber, condenser, cooling unit, evaporator and PLC. The stand is equipped with 6 thermocouples which can provide information about the temperature profiles, and the chamber pressure can also be monitored and registered.

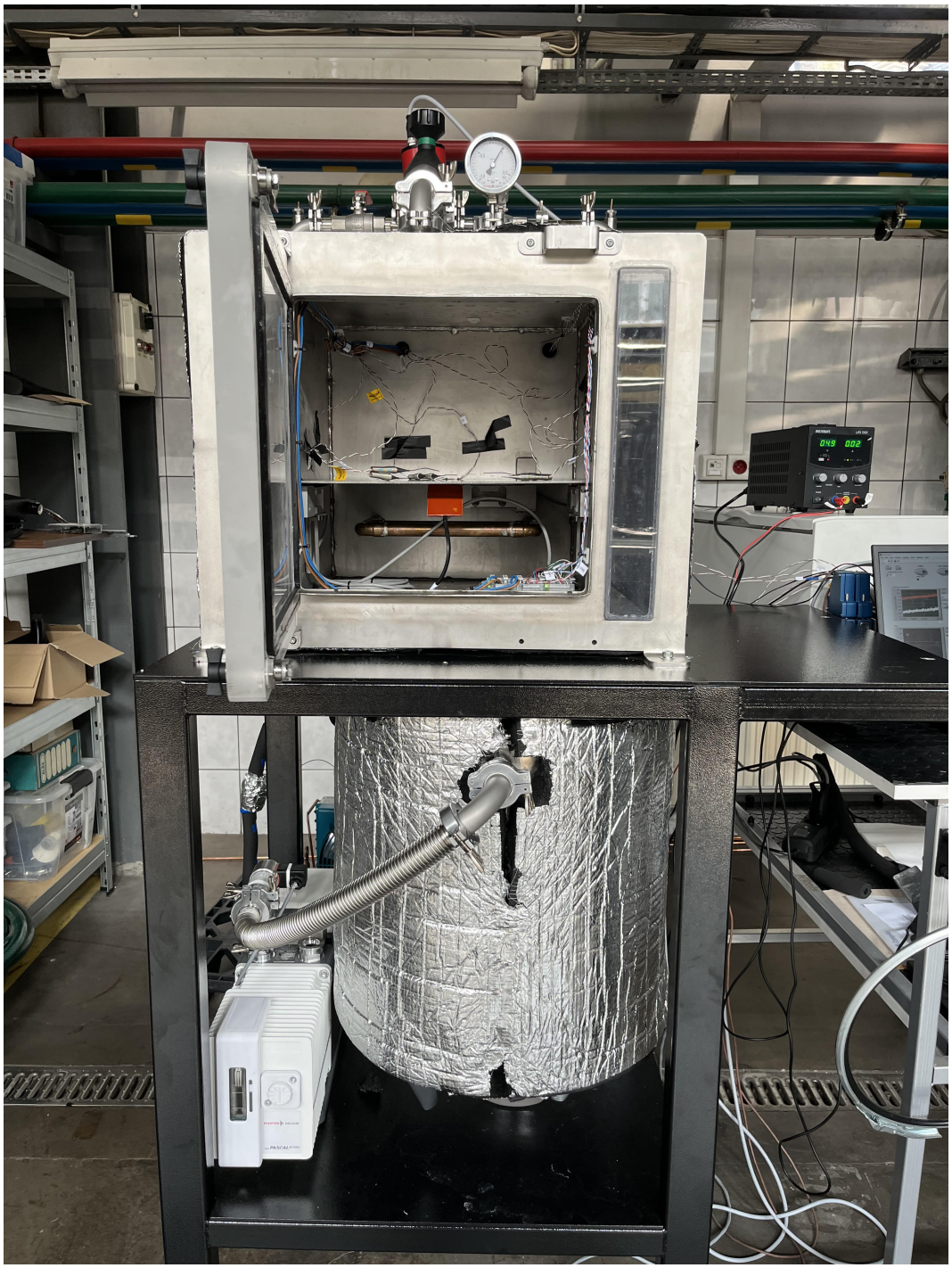

Figure 3.3.1: VacPCM vacuum chamber and condenser.

3.3.2 Sample

Analysed sample is a slice of potato visible in 3.3.2, with dimensions of 1 cm height and 2 cm radius. Potatoes were bought in a bulk from same distributor to reduce the likelihood of different batch of potatoes, and tests were conducted in the same day, to prevent different ripeness of samples.

Table 3.3.1: RS sponge characteristic [5]

Parameter	Value	Unit
Size	62.5 x 85 x 35	mm
Average pore diameter	60	μm
Water resistance	60 to 80	°
Porosity	88	%

3.3.2.1 Preparation

To prepare even potato slices, a sharp ring of 2 cm radius has been used to chop several slices out of each potato, which ensured even dimensions of each slice. The sample was cut out of the potato in such a way, so that the skin is not present. This is due to the high possibility that the skin may prohibit the water vapour from evaporating from the surface.

3.3.2.2 Measurements

Two thermocouples have been put into the sample from the side, one in the core of the potato, 0.5 cm from the top surface, and the other one in the surface, exactly 0.1 cm from the surface. As with the RS sponge sample described in Section 3.2.3.1, the thermocouple was not placed directly in the surface, but rather 0.1 cm deeper, to ensure that due to the shrinkage of the potato, the thermocouple would not simply fall out of the potato and provide readings of air temperature. Since the probe of thermocouple is significantly smaller than the testo915i used in experimental analysis of RS sponge, the accuracy of the position of the temperature sensor is much more precise. The potato slice was placed in the chamber in a way that can be seen in Fig. 3.3.2, along with other slices, which added up to 0.5 kg of food load. During each run, temperature of 3 potatoes was measured, with distinction of surface and core temperature.

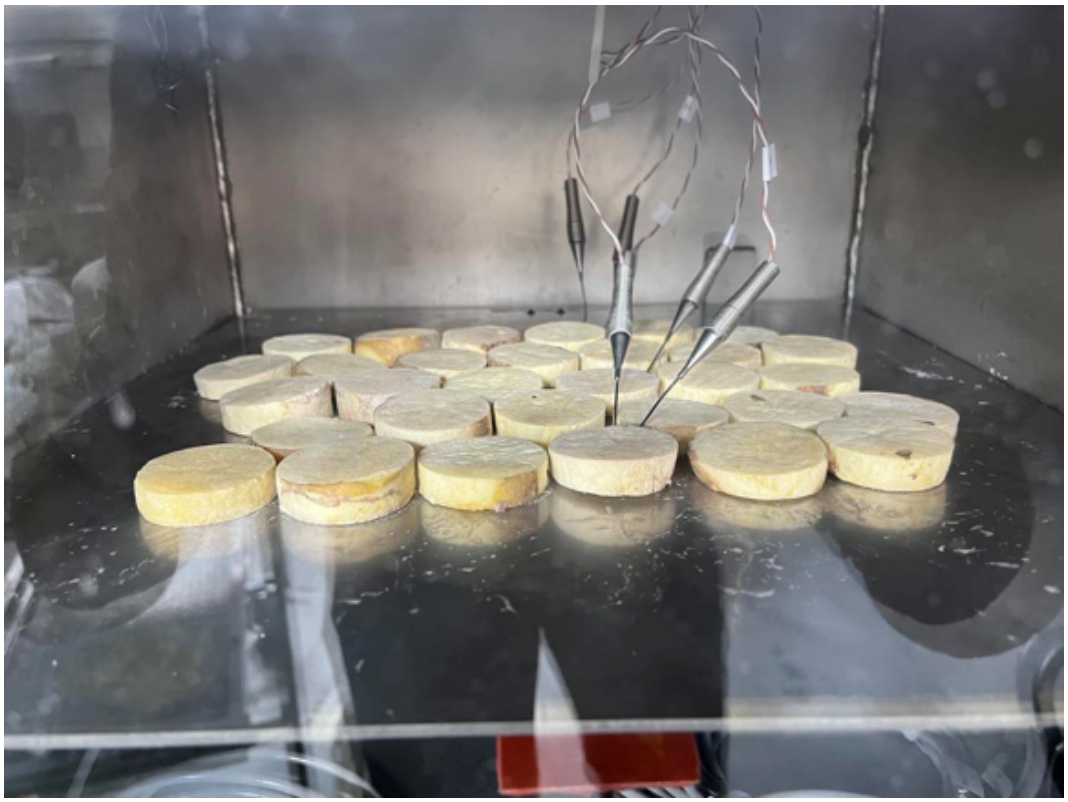

Figure 3.3.2: Placement of potatoes and thermocouples during experimental runs

3.4 Numerical model

3.4.1 Description and assumptions

The purpose of numerical model is to describe evaporation and sublimation of respectively water and ice caused by appropriately low surrounding pressure, and the resulting reduction of temperature.

In the first stage, pressure in the vacuum chamber is reduced from atmospheric pressure to pressure equal to equilibrium saturation pressure of water liquid at initial temperature of food product. During this stage no heat transfer or evaporation is occurring, but due to permeability of water, pressure gradient is formed, with highest value in the core and lowest close to the surface of food product.

In the second stage, as pressure in the vacuum chamber is now lower than equilibrium saturation pressure of water liquid, first evaporation begins on the surface of the product, and as the process goes by, pressure gradient moves to the core, thus causing evaporation region to move into the center of the product as well. Due to evaporation, saturation of water is now non-uniform in the product, leading to differences in permeability, causing even higher pressure gradient.

Third stage begins as soon as initial freezing temperature is achieved in any spot of the product, which causes liquid water to freeze. This effect is firstly seen on the surface of the food, and freezing front is slowly moving into the core of the product. With first appearance of ice, sublimation and evaporation are happening at the same time until all of the liquid water turns into ice. Assumptions of the preliminary model:

- Food sample domain is a porous zone made of solid material, and two phases filling the

pores: gas mixture consisting both air and water vapour, and water liquid.
- Porosity of the domain is isotropic.
- Vacuum chamber is not part of the model, and its pressure is set as a boundary condition on surface of the food product.
- Pressure drop of sample is caused by evacuation of water vapour through surface of the domain.
- Temperature in vacuum chamber is equal to temperature of food product.
- Temperature, pressure and volume fraction of each phase is uniform in the beginning of the process.

3.4.2 Geometry

3.4.2.1 water RS sponge

Three-dimensional symmetric cubic geometry with height of 3.5 cm, width of 4.25 cm and length of 6.25 cm has been developed based on RS sponge used in experimental part of the study. To reduce the computational demand of the CFD calculations, only half of the sponge was modelled, and symmetry has been assumed in the middle plane of the geometry, reducing the number of elements by half. This operation is allowed due to the symmetric shape of the sponge.

3.4.2.2 Potato slice

Potato slice has been modelled accordingly to the slices used in experimental tests, as a three-dimensional cylinder with height of 1 cm and 2 cm radius. As in Section 3.4.2.1, symmetry boundary condition has been introduced in the center plane along the height dimension to reduce the computational cost of calculations.

3.4.3 Mesh

3.4.3.1 Water RS sponge

Structural mesh has been created in ICEM CFD software. Due to the simple shape of geometry, no advanced mesh operations were needed to produce a high-quality structural mesh. To ensure an uniformity of each cell, number of elements along each edge was proportionally based on their length. Therefore, dimensions of each cell was approximately 1.75 mm, and the whole domain is made out of 14858 hexagonal elements. With the above operations, the quality of all elements is equal to 1.

Table 3.4.1: RS sponge geometry and mesh statistics

Dimension	Size [cm]	Number of elements along a dimension
Height	3.50	30
Width	4.25	36
Length	6.25	52

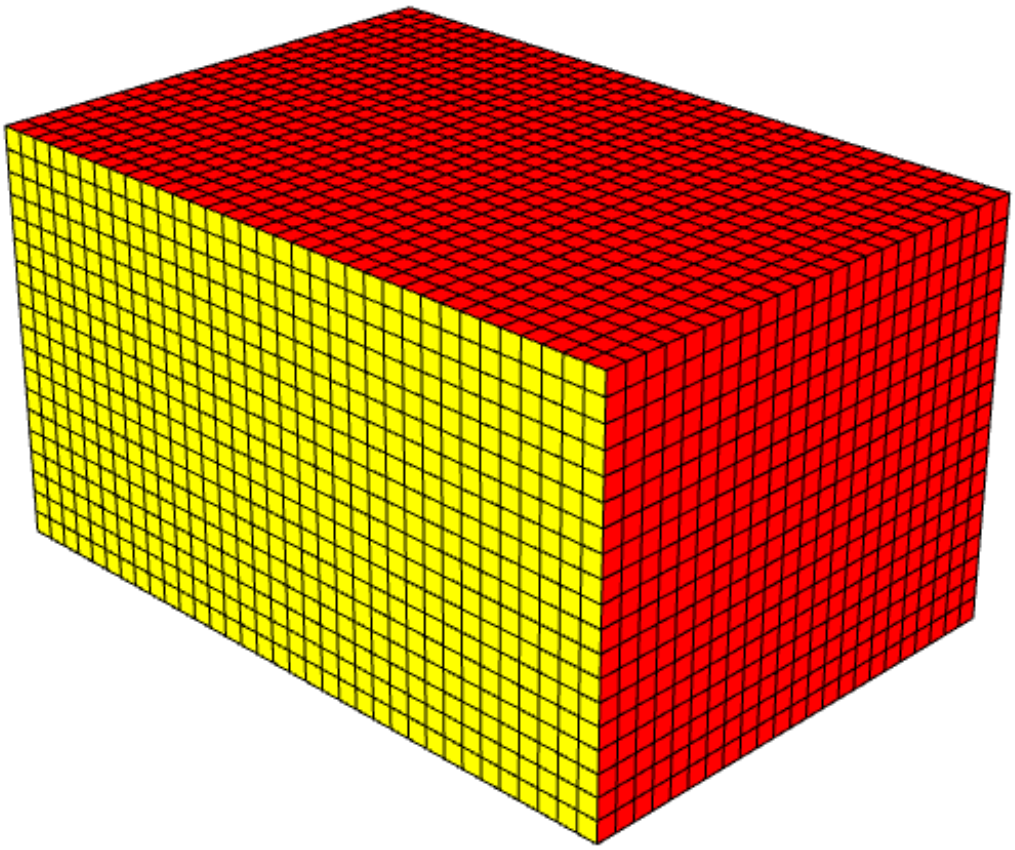

Figure 3.4.1: Isometric view on 3-D RS sponge geometry, with symmetry boundary condition (yellow) and pressure outlet (red).

3.4.3.2 Potato slice

To create a structural mesh of a cylinder geometry, a half O-grid type grid has been created using ICEM CFD software. It allows for a creation of structural hexa-element mesh that ensures better mesh quality. Whole mesh consists of 13868 elements, out of which 12754 cells are hexagonals and only 2016 cells are quads. The exact number of cells along the dimensions can be seen in Tab. 3.4.2 and Fig. 3.4.3. Out of 13868 elements, only 872 elements have quality of less than 0.5, 44 elements below 0.4, and just 16 below 0.2. The cells with quality less than 0.5 are shown in Fig. 3.4.3.2, and quality of whole domain is shown in Fig. 3.4.3.2 Therefore, the quality of mesh is assumed to be satisfactory for the multiphase model, especially considering the high computational cost of multiphase calculations.

Table 3.4.2: Potato slice geometry and mesh statistics

Dimension	Size [cm]	Number of elements along a dimension
Height	1.00	20
Diameter	4.00	32
A dimension	4.25	32
B dimension	4.25	16
C dimension	4.25	8

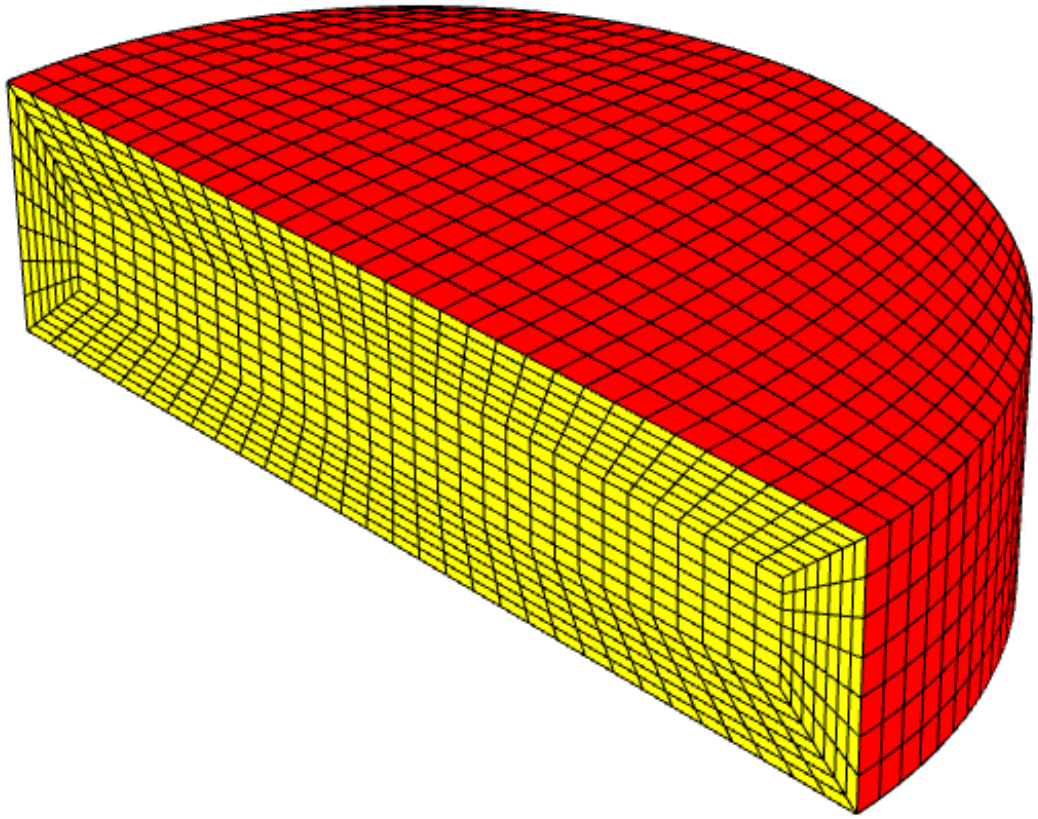

Figure 3.4.2: Isometric view on 3-D potato slice geometry, with symmetry boundary condition (yellow) and pressure outlet (red)

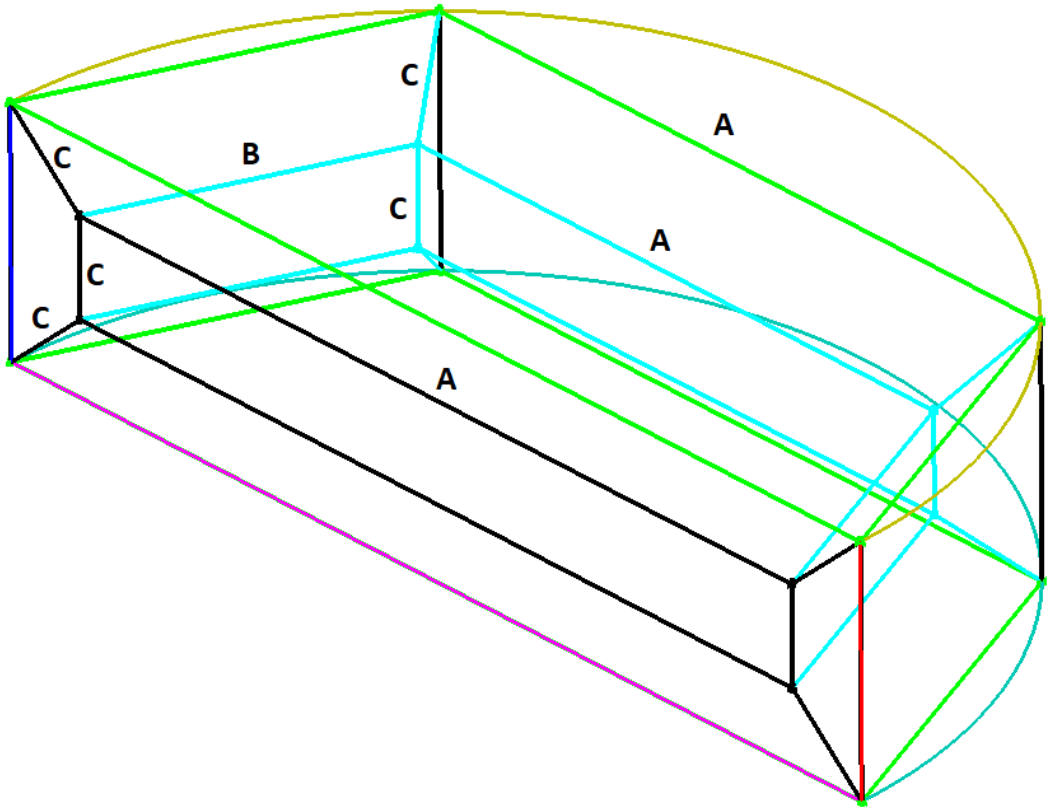

Figure 3.4.3: Number of cells along the dimensions of half O-grid potato slice mesh

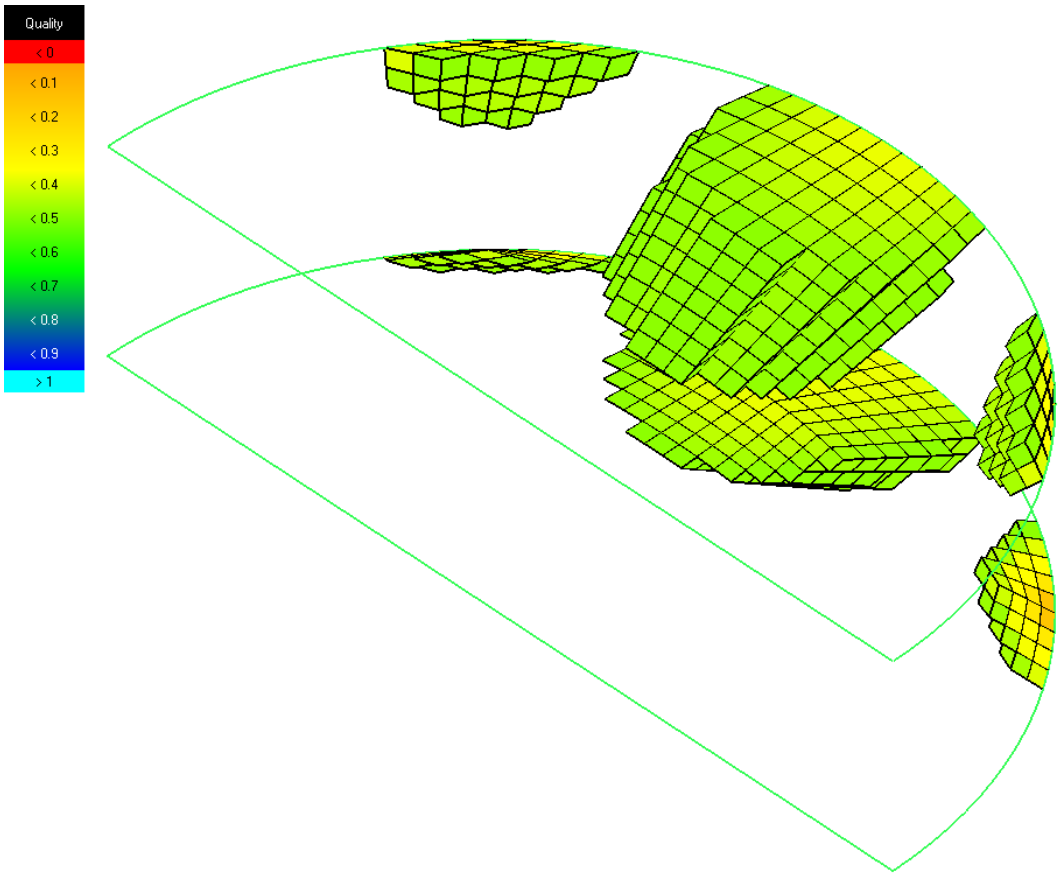

Figure 3.4.4: Cells that exhibit potato slice mesh quality less than 0.5

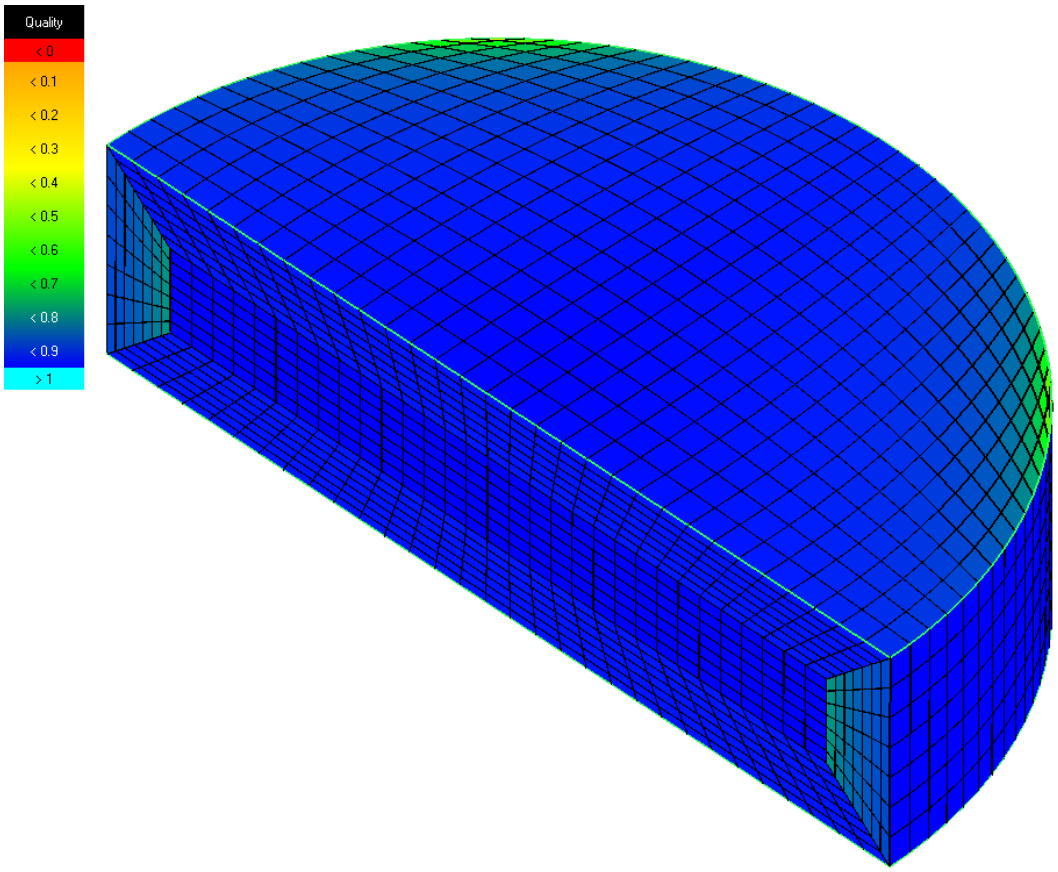

Figure 3.4.5: Quality of 3-D potato mesh

3.4.4 Computational domain

Computational domain is a porous zone made of solid material and multi-phase fluid consisting liquid water and gas mixture containing vapour water and air. Multiple time step sizes were tested for the calculations, and time step with size of 0.01 second was selected. It proved to be the highest time step that ensured solution stability, with Courant number, which describes amount of cells that flow advances during one time step, not exceeding 1 over the whole duration of calculation. Choosing lower time step could provide more accurate results, but would multiply the required computational cost, with diminishing increase in accuracy.

3.4.4.1 Multi-phase model

To simulate liquid water and gas mixture composed of water vapour and air, multiphase model was introduced to the model. It allows for coexistence of 2 and more phases in one domain, each with separate physical and thermal properties. Presence of this mathematical model is crucial to simulate the water evaporation and different thermal and physical properties of gaseous and liquid water, such as density, thermal diffusivity, permeability etc.

3.4.4.2 Viscous model

Due to the very slow velocity of the flow within the product, flow is assumed to be laminar, and no turbulence models have to be applied.

3.4.4.3 Porous model

Introduction of porous model allows for simulating porous material of the sample. As RS sponge is a material of 88% porosity **??**, meaning that just 12% of the volume is the actual sponge, while water-filled pores occupies 88% of the volume, and in case of a potato slice, the porosity of the material is assumed to be equal to 70%, meaning that 30% of the domain is solid or non-porous. In case of mathematical model, porous model adds a momentum sink to governing momentum equation, which results in reduction of velocity and simulates the pressure loss in the flow due to resistances of the solid material and liquid media flowing in the pores.

3.4.5 Governing equations

3.4.5.1 Momentum equation

Darcy's law

In case of laminar flows in porous media, pressure drop is given by Darcy's law, that describes the flow rate in the porous zone by the pressure gradient, fluid's viscosity and permeability of the media. [54]:

$$\nabla p = -\frac{\mu}{\alpha} u \tag{3.1}$$

where ∇p is the pressure drop $[Pa]$, μ is viscosity $[Pas]$ and α is permeability $[m^2]$.

Momentum source term

Porous media adds to flow equations a momentum source term, in form of Darcy's viscous loss term and an inertial loss term:

$$S_{in} = -\left(\sum_{j=1}^{3} D_{ij}\mu u_j + \sum_{j=1}^{3} C_{ij}\frac{1}{2}\rho|u|u_j\right) \tag{3.2}$$

which in multi-phase domain translates to:

$$S_{in} = -\left(\frac{\mu}{\alpha}u_i + C_2\frac{1}{2}\rho|u|u_i\right) \tag{3.3}$$

where S_i is the source term for ith momentum equation,D and C are prescribed matrices which translate to $D = 1/\alpha$ and $C = C_2$.

Physical velocity

While using porous media model, fluent calculates superficial velocity which is dependent on volumetric flow rate, and is equal to physical velocity multiplied by porosity [54]:

$$u_{superficial} = \phi u_{physical} \tag{3.4}$$

where ϕ is the porosity of the media [%].

Using porous model also allows for Physical Velocity Porous Formulation, which includes porosity in transport equations and is more accurate compared to superficial formulation [54]. This gives the resulting governing equation:

$$\frac{\partial}{\partial t}(\phi\varphi_i\rho_i u_i\Phi_i) + \nabla\cdot(\phi\varphi_i\rho_i u_i\Phi_i) = \nabla\cdot(\phi\Gamma\nabla\Phi_i) + S_{\Phi,i} \tag{3.5}$$

where φ is the volume fraction $[m^3m^{-3}]$, Φ is a general scalar, Γ is the scalar diffusion coefficient and $S_{\Phi,i}$ is the source term. Taking to account above factors, the momentum equation takes the form below: The momentum equation for liquid water [54]:

$$\begin{aligned}\frac{\partial}{\partial t}(\phi\rho_w u_w\varphi_w) + \nabla\cdot(\phi\rho_w {u_w}^2\varphi_i) = \\ -\phi\varphi_w\nabla\cdot(p-p_c) + \phi\varphi_w\rho_w - (\phi^a{\varphi_w}^a\frac{\mu_w u_w}{K_{r,w}K} + \phi^b{\varphi_w}^b\frac{C_2\rho_w {u_w}^2}{2})\end{aligned} \tag{3.6}$$

The momentum equation for gas mixture[54]:

$$\begin{aligned}\frac{\partial}{\partial t}(\phi\rho_g u_g\varphi_g) + \nabla\cdot(\phi\rho_g {u_g}^2\varphi_i) = \\ -\phi\varphi_g\nabla\cdot(p-p_c) + \phi^a{\varphi_g}^a\rho_g - (\phi\varphi_g\frac{\mu_g u_g}{K_{r,w}K} + \phi^b{\varphi_g}^b\frac{C_2\rho_g {u_g}^2}{2})\end{aligned} \tag{3.7}$$

where p is pressure $[Pa]$, p_c is the capillary pressure for the wetting phase $[Pa]$, K_r is the relative permeability $[m^2]$ and K is the intrinsic permeability $[m^2]$, and a and b are coefficients fitted based on experimental data.

3.4.5.2 Mass transport equation

Transport of mass is described by a porous media multi-phase model with gas mixture containing vapour water and air, and liquid water as two separate phases. The continuity equation for liquid water [37, 54]:

$$\frac{\partial}{\partial t}(\phi\rho_w\varphi_w) + \nabla\cdot(\phi\rho_w u_w\varphi_w) = R_{evap} \tag{3.8}$$

The continuity equation for gas mixture is as follows [37, 54]:

$$\frac{\partial}{\partial t}(\phi\rho_g\varphi_i) + \nabla\cdot(\phi\rho_g u_g\varphi_i) = R_{evap} \tag{3.9}$$

where R_{evap} is the evaporation rate from liquid water to vapour water [55]:

$$R_{evap} = K_{evap}\left(a_w p_{sat} - p\right)\frac{M_v\phi\varphi_g}{RT} \tag{3.10}$$

where K_{evap} is the evaporation rate coefficient $[1s^{-1}]$, a_w is the water activity, p_{sat} is saturation pressure of liquid water $[Pa]$ in local temperature T $[K]$, M_v is molar mass of water vapour $[kgkmol^{-1}]$ and R is a gas constant $[kJK^{-1}kmol^{-1}]$.

3.4.5.3 Energy equation

Thermal conductivity

The effective thermal conductivity is calculated based on composition of the fluid in the sponge. The effective thermal conductivity of medium is calculated using Levy's formula Eq. 2.7, 2.8, 2.9 mentioned in Section 2.3.2 The effective thermal conductivity of porous medium is a result of thermal conductivity of both fluid phases and solid material of which porous zone is made of:

$$k_{eff_{pr}} = \phi \left(k_{eff_w}\varphi_1 + k_{eff_g}\varphi_2\right) + (1-\phi)k_s \tag{3.11}$$

where $k_{eff_{pr}}$ is the effective thermal conductivity of the porous medium $[Wm^{-1}K^{-1}]$, k_{eff} is the effective thermal conductivity of each phase $[Wm^{-1}K^{-1}]$ and k_s is the thermal conductivity of solid media $[Wm^{-1}K^{-1}]$.
Energy equation [44, 56]:

$$\rho\frac{\delta H}{\delta t} = \nabla\left(\frac{k_{eff}}{c}\nabla H\right) \tag{3.12}$$

where H is the enthalpy $[kJ]$ and c is the specific heat $[kJkg^{-1}K^{-1}]$.
Boundary condition:

$$k_{eff}\nabla T = L \cdot K_{evap}(p_{sat} - p_g) \tag{3.13}$$

where L is the latent heat of evaporation $[kJkg^{-1}]$.
Using enthalpy:

$$\frac{k_{eff}}{c}\nabla H = L \cdot K_{evap}(p_{sat} - p_g) \tag{3.14}$$

3.4.6 Input parameters

All of the input parameters are listed in Tab. 3.4.4
Freezing point

Freezing point of the product has been assumed to be equal to freezing point of pure water:

$$T_{if} = -\frac{1}{\varphi_w}\left(4.66\varphi_{other} + 46.4\varphi_{ash}\right) \tag{3.15}$$

Evaporation and sublimation rate

Evaporation rate is driven by the difference between the local equilibrium saturation pressure corresponding to current temperature of liquid and vapour pressure of liquid water [31, 55]:

$$R_{evap} = K_{evap}(a_w \cdot p_{sat} - p_v)\frac{\phi S v M_v}{RT} \tag{3.16}$$

where R_{evap} is evaporation rate $[kgm^{-3}s^{-1}]$ and K_{evap} is evaporation constant, fitted based on experimental data of certain foods.

Saturation

Water saturation and water vapour saturation are defined as the phase volume fraction in the pore, or in the porous model as a volume fraction of a phase in a cell.

Permeability

Permeability of the media is calculated based on saturation of each phase, their absolute permeability, and experimentally fitted Corey exponent [54], assumed in this study to be 1:

$$\alpha = K_{r,i}\bar{S}_i^{ni} \tag{3.17}$$

where $K_{r,i}$ is the reference ith phase relative permeability $[m^2]$, $\bar{S}_i^{ni}$ is the normalized saturation in the ith phase, and ni is the Corey exponent for the ith phase.

Porosity

Porosity is defined as the volume fraction which is occupied by fluid phases in radial (r) and axial (z) coordinates [37]:

$$\phi(r,z) = \frac{1}{\delta V}\sum_i \delta V_i \tag{3.18}$$

where i represents an ith phase, and δV is the whole volume of domain $[m^3]$, and δV_i is volume of ith phase $[m^3]$.

Pressure in the vacuum chamber

The pressure in the vacuum chamber is set to the pressure profile achieved during experimental tests.

Table 3.4.3: Input parameters of a RS sponge case

Parameter	Symbol	Value	Unit	Source
Initial temperature	T_0	279.15	K	experimental data
Initial chamber pressure	P_{ch}	101325	Pa	experimental data
Initial freezing point	T_{if}	273.65	K	experimental data
Density of water	ρ_w	998	kgm^{-3}	–
Density of gas	ρ_w	Ideal gas	kgm^{-3}	–
Thermal conductivity of water	k_w	Eq. 2.7	$Wm^{-1}K^{-1}$	[46]
Thermal conductivity of vapour	k_w	0.026	$Wm^{-1}K^{-1}$	[57]
Thermal conductivity of air	k_a	0.026	$Wm^{-1}K^{-1}$	[57]
Effective thermal conductivity	$k_{eff_{pr}}$	Eq. 3.11	$Wm^{-1}K^{-1}$	[57]
Viscosity of water	μ_w	$9.27x10^{-4}$	$Pa{\cdot}s$	[58, 31]
Viscosity of vapour	μ_v	$1.80x10^{-5}$	$Pa{\cdot}s$	[58, 31]
Viscosity of air	μ_a	$1.80x10^{-5}$	$Pa{\cdot}s$	[58, 31]
Effective specific heat above freezing	c_{unf}	Eq. 2.1	$Jkg^{-1}K{-}1$	[44]
Effective specific heat below freezing	c_f	Eq. 2.2	$Jkg^{-1}K{-}1$	[44]
Absolute permeability of water	α_w	$1x10^{-15}$	m^2	[31]
Absolute permeability of gas	α_g	$1x10^{-11}$	m^2	Assumed
Initial saturation of water	S_{w_in}	0.90	—	Assumed
Residual saturation of water	S_{w_res}	0.08	—	[55, 31]
Residual saturation of gas	S_{g_res}	0.01	—	Assumed
Evaporation constant	K_{evap}	800	—	Assumed

Table 3.4.4: Input parameters of a potato slice case

Parameter	Symbol	Value	Unit	Source
Initial temperature	T_0	279.15	K	experimental data
Initial chamber pressure	P_{ch}	101325	Pa	experimental data
Initial freezing point	T_{if}	271.65	K	experimental data
Density of water	ρ_w	998	kgm^{-3}	–
Density of gas	ρ_w	Ideal gas	kgm^{-3}	–
Thermal conductivity of water	k_w	Eq. 2.7	$Wm^{-1}K^{-1}$	[46]
Thermal conductivity of vapour	k_w	0.026	$Wm^{-1}K^{-1}$	[57]
Thermal conductivity of air	k_a	0.026	$Wm^{-1}K^{-1}$	[57]
Effective thermal conductivity	$k_{eff_{pr}}$	Eq. 3.11	$Wm^{-1}K^{-1}$	[57]
Viscosity of water	μ_w	$9.27x10^{-4}$	$Pa{\cdot}s$	[58, 31]
Viscosity of vapour	μ_v	$1.80x10^{-5}$	$Pa{\cdot}s$	[58, 31]
Viscosity of air	μ_a	$1.80x10^{-5}$	$Pa{\cdot}s$	[58, 31]
Effective specific heat above freezing	c_{unf}	Eq. 2.1	$Jkg^{-1}K{-}1$	[44]
Effective specific heat below freezing	c_f	Eq. 2.2	$Jkg^{-1}K{-}1$	[44]
Absolute permeability of water	α_w	$1x10^{-15}$	m^2	[31]
Absolute permeability of gas	α_g	$1x10^{-11}$	m^2	Assumed
Initial saturation of water	S_{w_in}	0.80	—	Assumed
Residual saturation of water	S_{w_res}	0.08	—	[55, 31]
Residual saturation of gas	S_{g_res}	0.01	—	Assumed
Evaporation constant	K_{evap}	150	—	Assumed

CHAPTER
FOUR

RESULTS AND DISCUSSION

4.1 Experimental Vacuum freezing of the RS sponge

4.1.1 µWaveVac0250

Fig. 4.1.2 and Tab. 4.1.2 show temperature and pressure profiles of 6 repetitions of RS sponge vacuum freezing in µWaveVac0250. As mentioned in Section 3.2.3.1, temperature was measured at 3 different locations of the sample to gain better understanding of the temperature gradients existing throughout the vacuum freezing process.

4.1.1.1 Temperature

Temperature of RS sponge during the process of vacuum freezing varies highly depending on temperature sensor location, with core being the least cold and surface being the coldest. The difference between coldest and least cold measured points on average reached as high as 20 °C, and was always measured just before the core started to freeze. The high difference in temperature reduction rate is caused by high volume to surface ratio of the sponge, and very high pressure reduction rate. Average temperature drop listed in Tab. 4.1.2 shows that on average temperature in the core was being reduced 0.6 times slower as at the surface, and 0.7 times slower than in the middle. It must be noticed, that the temperature reduction rate in the core is 5.4 times faster after the freezing, with 0.03 °C/minute, when compared to temperature reduction before it reaches freezing point, equal to 0.07 °C. This can be explained by the temperature plateau which is visible in the Fig. 4.1.2 at the $\tau = 1000$ seconds.

4.1.1.2 Pressure

Pressure decrease rate in the µWaveVac0250 apparatus was equal to 52500 Pa/minute in the first 115 seconds, and 9.5 Pa/minute since the 115 second to the end of the process. Very high decrease rate of pressure in the first 115 seconds resulted in high temperature drop rate in the surface, before the temperature in the core started to drop. High pressure reduction rate influences the time required for the product to reach desired temperature, but also creates unfavourable temperature gradients, which was the case in experimental analysis of vacuum freezing performed in µWaveVac0250 device, resulting in difference

between core and surface temperature of 18.3 °C at $\tau = 990$ seconds, which be seen in Fig. 4.1.2. When taking into account the importance of freezing uniformity or at least if high temperature gradients need to be avoided, pressure reduction rate should be controlled by a valve. In scenario where pressure drop rate is gradually adjusted, temperature across the product is much more uniform due to the fact that the difference of reduction rate of temperature inside the product and in the surface is lower.

4.1.1.3 Supercooling and phase change plateau

Due to the large heat capacity of the condenser, very low temperature of the evaporator coil, and perhaps very high efficiency of vacuum pumps, no supercooling nor nucleation can be seen in the temperature readings. No increase in temperature during phase change can be fairly explained when its occurring the surface, because the released latent heat could be very quickly transferred and absorbed to the condenser, however, an increase in temperature in the range of phase change temperature cannot be seen also in the middle point, which was measured in between the core and the surface, spaced 0.45 cm from each. It should be considered, that the extremely fast cooling rate caused by the very rapid pressure drop, and very large in both size and heat capacity condenser, could be such a great factor in respectively reducing temperature and absorbing latent heat, that the latent heat of evaporation is also absorbed by the condenser. However, the temperature plateau in the core of the product can be seen in 4.1.2, and its occurrence could be explained by the fact, that moisture at surface of the product has already went through nucleation and phase change, so the mechanism for freezing in the rest of the body is now the formation of ice crystals on the moving freezing front. Nevertheless, temperature of the liquid water could not be reduced below freezing point, and will only do so if is in contact with freezing front. Therefore, the temperature will remain equal to initial freezing temperature for as long as there is no ice in contact with it. With the above being mentioned, it may be possible, that the surface of the sponge dried under the heavy loss of mass, that can be seen in Fig. 4.1.1, and no or little moisture was between the measured location and the surface, resulting in released latent heat getting absorbed by the condenser.

4.1.1.4 Mass loss

During the experimental tests of vacuum freezing of RS sponge, ± 22.4% of whole moisture evaporated from the sponge. The highest mass loss can be observed in the first stage of vacuum freezing - when theoretically no evaporation should occur, due to the chamber pressure being higher that the saturation pressure of water, and in the second stage, which is cooling. The high mass loss during the 1^{st} stage of vacuum freezing, where no evaporation should occurr, could be explained by the water spilling out of the sponge due to the rapid pressure reduction rate. A plastic box was placed underneath the sponge, so the spilled water should have ended up in the box, but it is possible that the spilled water flowed on top of the mesh that was on top of the box, and ended up out of the box. The reason could also be that due to the rapid pressure reduction in the chamber, the scale readings show a reduction of mass, even though the weight remain unchanged.

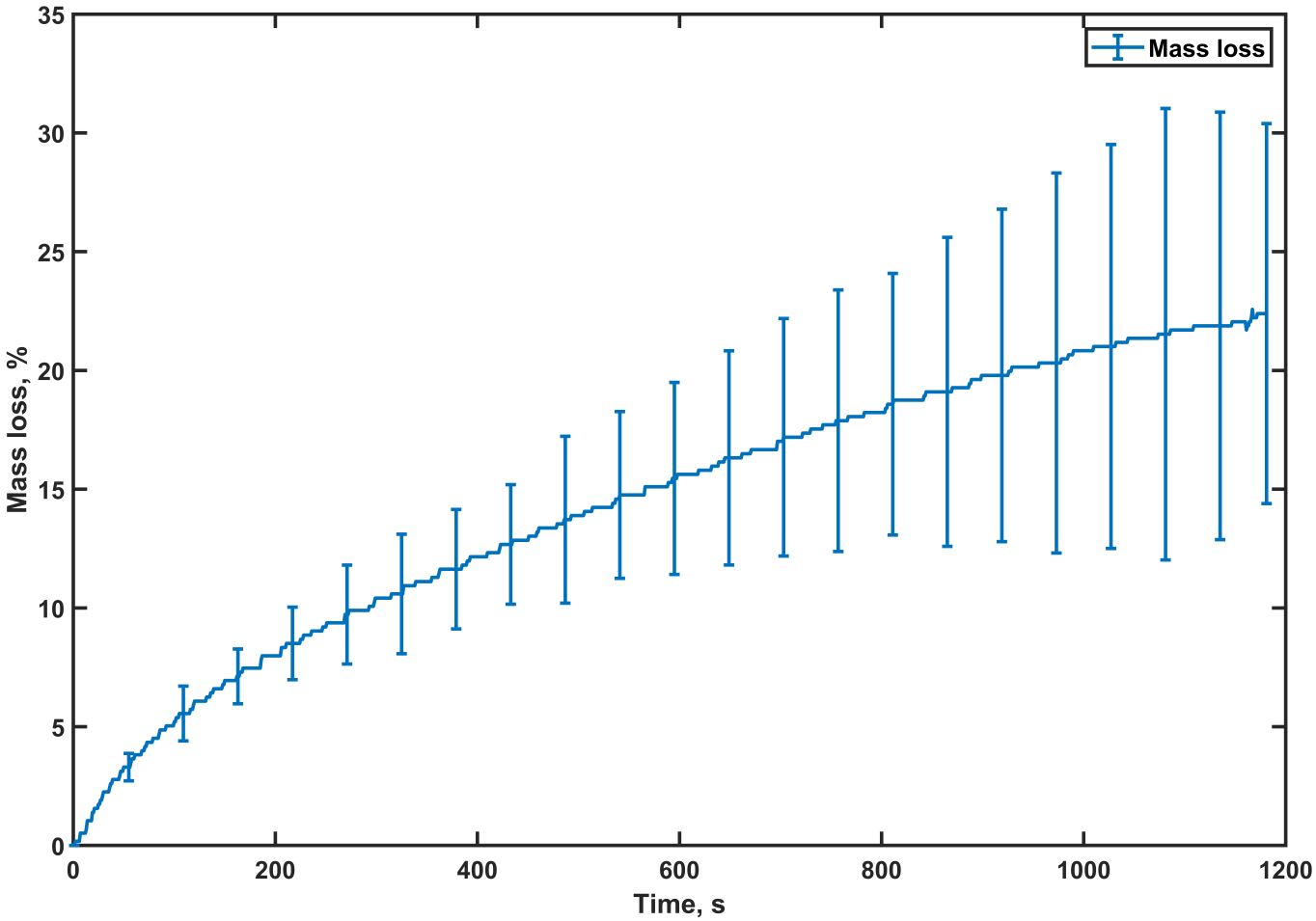

Figure 4.1.1: Mass lost during vacuum freezing in µWaveVac0250

4.1.1.5 Statistics

Due to the lab temperature being over 18 degrees higher than initial temperature of the sponge, standard deviation of temperature at the beginning of the process is between $\sigma_{core} = 0.51$ °C and $\sigma_{surface} = 0.68$ °C depending on the measured point. Highest σ at surface can be seen at $\tau = 125$ seconds, and can be explained by the fact that the evaporation process had just barely started, resulting in rapid temperature drop, so just a few seconds of evaporation delay between samples can cause relatively high deviations of temperature at that time. Standard deviation of temperature measured in the core of the product until freezing point is caused mostly by the initial temperature difference. This is due to the very slow temperature reduction in the core of the product until the end of the plateau. As soon as water starts to freeze in this point, the temperature deviations escalates because of the most rapid temperature reduction across any point of the product and any time of the process. Average standard deviations are listed in Section 4.1.2, and do not exceed $\sigma = 1.66$ °C. The divergence in the measured temperatures in each test are also caused by inevitable differences in the exact position of measuring device, since even small misplacement in depth, width and height affects the readings significantly. Pressure drop rate in each repetition was almost exactly the same, with highest standard deviation of 8%, which is equal to ± 5 Pa difference at the level of 60 Pa and and therefore the standard deviation of pressure can be neglected.

Table 4.1.1: Standard deviations of temperature during the µWaveVac0250 vacuum freezing process of water RS sponge

Measured position of the RS sponge	Average $\frac{dT}{d\tau}$	Average STD	Initial STD	End STD
Core	0.016	0.94	0.56	5.67
Middle	0.023	1.66	0.51	2.33
Surface	0.027	1.22	0.68	1.41

4.1.2 LyoCube

Results of vacuum freezing tests performed in LyoCube device are very much different when compared with µWaveVac0250 results shown in Section 4.1.1. Pressure drop rate is significantly lower, since the system is equipped with just one vacuum pump, compared to µWaveVac0250's three vacuum pumps. With process lasting over 66 minutes, the temperature at the surface is above -4 °C, and in the core above -1 °C, which is over 3 times longer to reach surface temperature of -25 °C in µWaveVac0250 apparatus. This is caused by slower pressure drop rate, and lack of cooling system which results in higher lowest pressure limit in the chamber, since the absence of evaporator coil prevents the evaporated moisture in the chamber from resublimating, so its present in the chamber until it eventually gets sucked by the vacuum pump.

4.1.2.1 Temperature

Temperature profiles in the are much different from the µWaveVac0250 results, even though it is the same process. In this case, temperature across all measured points drops well below freezing point and at the exact same time it undergoes nucleation in whole volume of the product. The temperature increases and is maintained at a plateau until it eventually starts to drop again, starting from the surface and eventually deeper in the product. Depending on the location, plateau lasts from approximately 500 seconds in the surface, to 3000 seconds in the core. If cooling unit was utilised in this system, the released latent heat of freezing would be absorbed by the evaporator, thus reducing the time of plateau or even removing this effect completely, depending on location in the product.

Table 4.1.2: Standard deviations of temperature during the LyoCube vacuum freezing process of water RS sponge

Measured point	Average $\frac{dT}{d\tau}$	Average STD	Initial STD	End STD
Core	0.0015	0.32	0.57	0.63
Middle	0.0018	0.53	0.35	0.21
Surface	0.0027	0.45	0.42	1.20

4.1.2.2 Mass loss

The mass loss was checked after the process, due to the lack of built-in scale inside the LyoCube in the system. The average mass loss of the process was 15.6%. When compared to the vacuum freezing experiments in µWaveVac0250, the mass lost in LyoCube is just 4.4% lower, and while the process in LyoCube was 46 minutes longer, the average

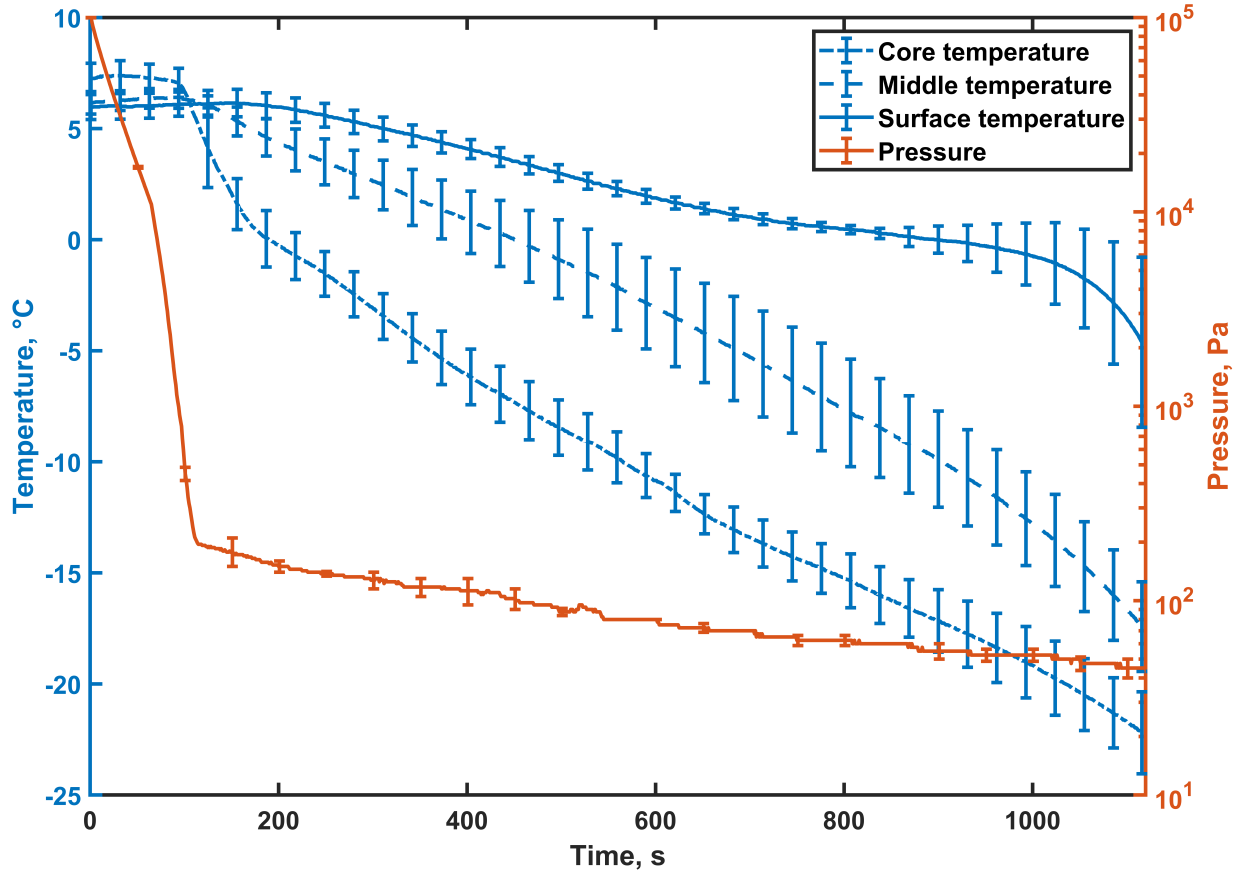

Figure 4.1.2: Temperature profiles of vacuum freezing of water RS sponge in µWaveVac0250

temperature drop was equal to 8 °C during 4000 seconds of vacuum freezing process, opposed to 20 °C in 1200 seconds in µWaveVac0250 device. Mass loss should increase with higher duration of the process and temperature reduction. Also, the temperature plateau that occurred in LyoCube means that the moisture in the sponge kept evaporating even though the temperature was not being reduced.

4.1.2.3 Statistics

As in Section 4.1.1.5, the ambient temperature of the lab was 18 °C higher than the initial temperature of the water RS sponge, so the initial temperature was the highest in the surface of the product, since the warm air increased the surface temperature of the sponge. The difference between initial temperature of different measured points in the sponge was equal to 0.5 °C, and he initial standard deviation of averaged cases was between σ = 0.1 °C in the middle and in the core, and σ = 0.4 °C in the surface of the sponge. The highest standard deviation of σ = -4.55 °C can be observed in τ = 1116 seconds. The average standard deviation of analysed processes did not exceed 0.53.

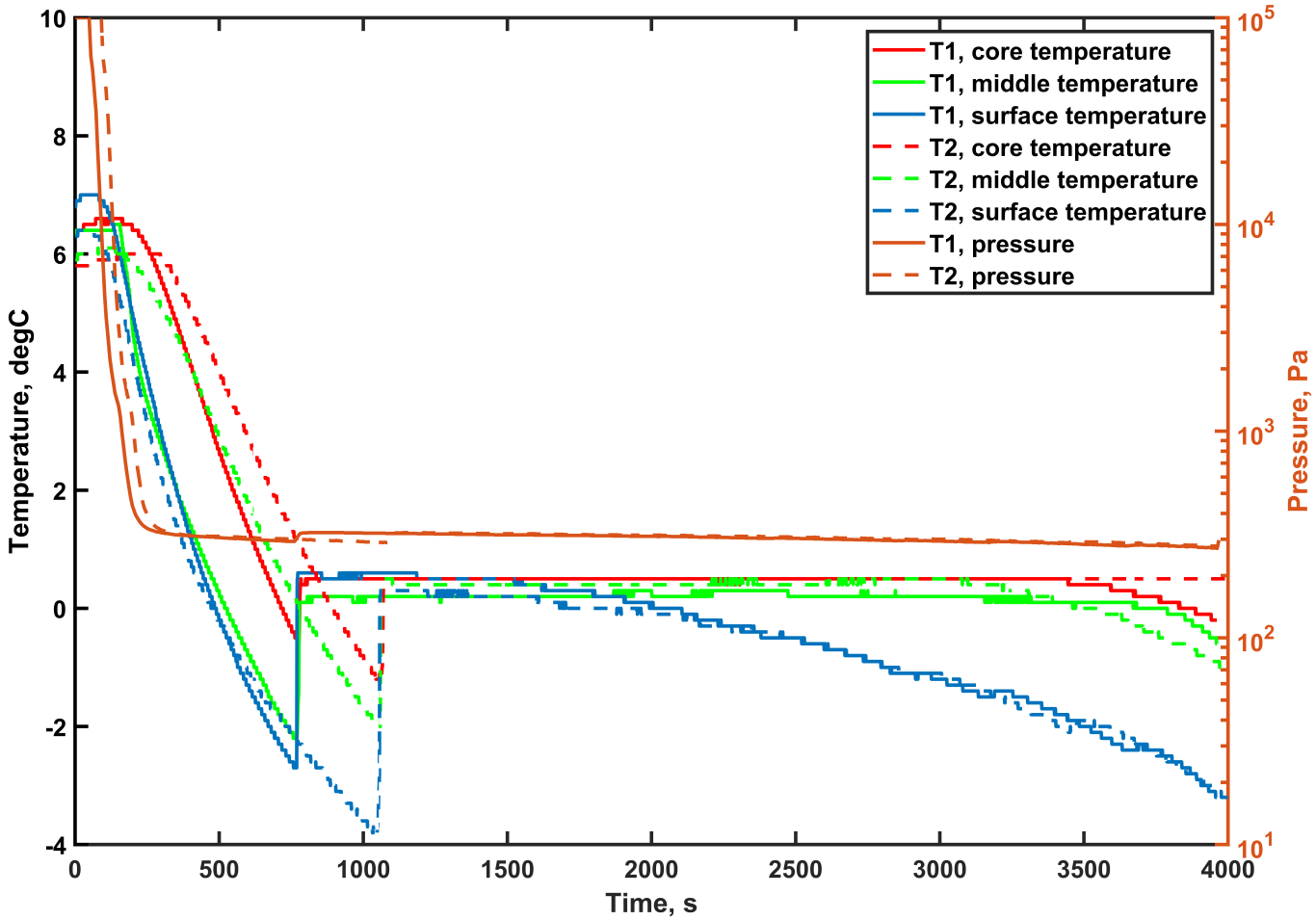

Figure 4.1.3: Temperature profiles of Vacuum freezing of water RS sponge in LyoCube device

4.1.3 Oil

To study the influence of the vacuum pump oil on the time of the vacuum freezing process, two runs were performed on LyoCube device, one with oil that was already used in over 20 runs, and one with just poured unused oil. It needs to be mentioned, that LyoCube setup has no cooling unit in the setup, which results in all of the evaporated moisture getting sucked in and absorbed by the vacuum pump oil. In case of apparatus with cooling unit, the amount of vapour getting into the pump and then condensing is greatly reduced. Temperature was only measured in the core of the sponge, since temperature profiles were not of any interest. With old oil, 780 seconds of pumping time was required for chamber to reach 360 Pa, while with using new oil the time was reduced to 290 seconds, which is over 2.5 times faster. It's easily visible in Fig. 4.1.5, that time of nucleation between two cases is delayed by a significant amount of time, with old oil needing 2250 seconds, and fresh oil just 1020 seconds, which is over twice as fast.

That analysis shows how important it is to prevent vapour from the vacuum pump, and exchange the costly vacuum pump oil if decrease in efficiency is observed. It affects the effectiveness of the pump, thus increases time and energy required for the process to finish, so exchanging the costly vacuum pump oil after x completed runs may reduce the overall cost of running the process.

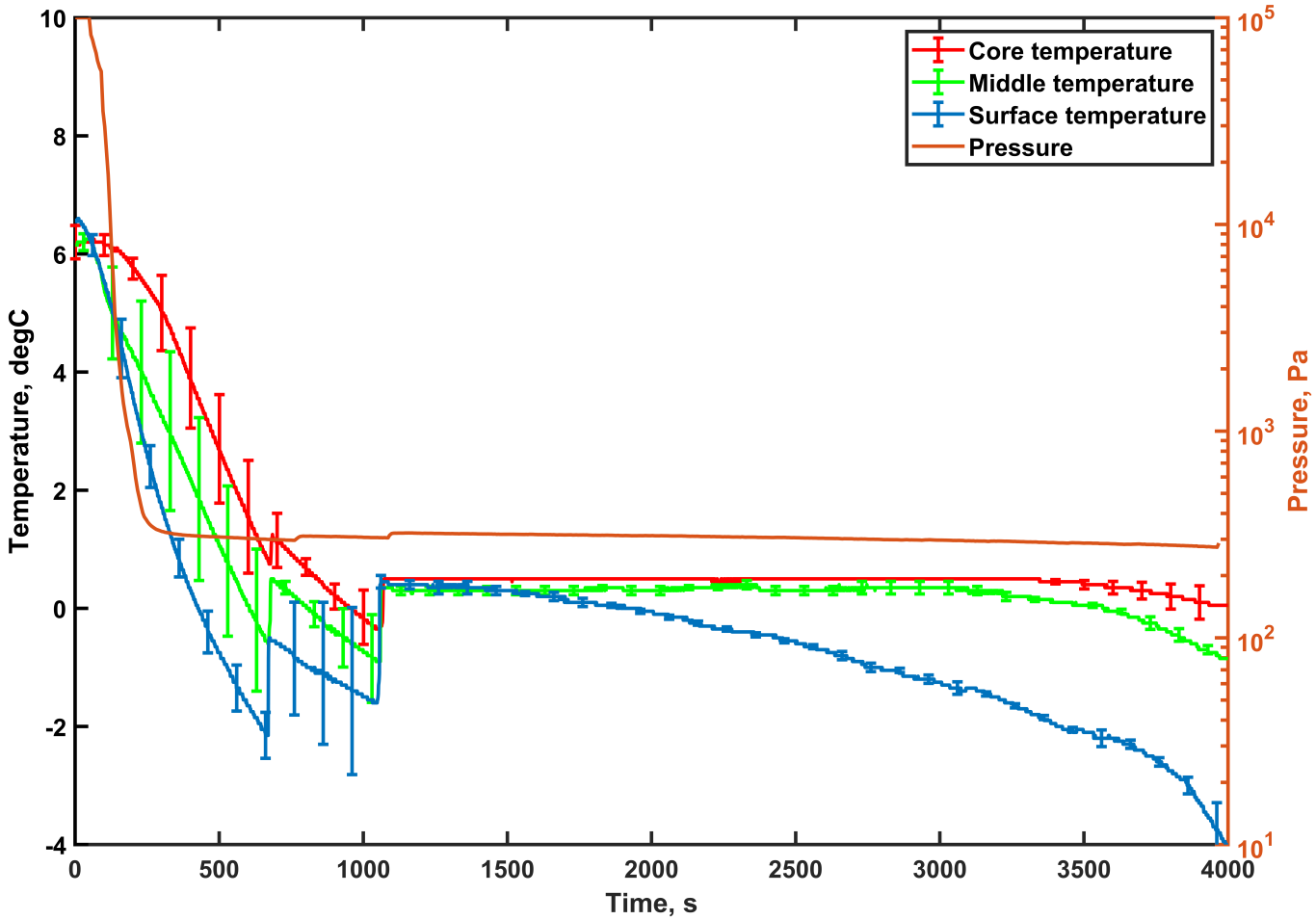

Figure 4.1.4: Averaged temperature profiles of vacuum freezing of water RS sponge in LyoCube device

4.1.4 Influence of refrigeration system

Cooling system proved to be a crucial aspect of vacuum freezing system, that has an outstanding influence on variety of vacuum freezing process properties, such as pressure, temperature, and resulting time, which can be deducted from the difference in results from µWaveVac0250 4.1.2and LyoCube 4.1.4. Lack of cooling system greatly reduced pressure drop rate and increased low pressure limit, which in effect decreased cooling and freezing rate, and in consequence multiplied the time required to finish the vacuum freezing process. Very importantly, sufficient cooling system protects vacuum pump from damage and reduction of pumping speed studied in Section 4.1.3, caused by condensing vapours that would get sucked into the pump if not the evaporator in which vapours condensate.

4.1.5 Pressure

To check the influence of the pressure on the process, two vacuum freezing runs were performed, with temperature measured in the core of the product. In first instance, the vacuum pumps were working during the whole process, but the valve which is supposed to break the vacuum in the chamber after the process was slightly opened, to increase the pressure in the chamber. By that, pressure was maintained at 450 Pa up to 900 seconds

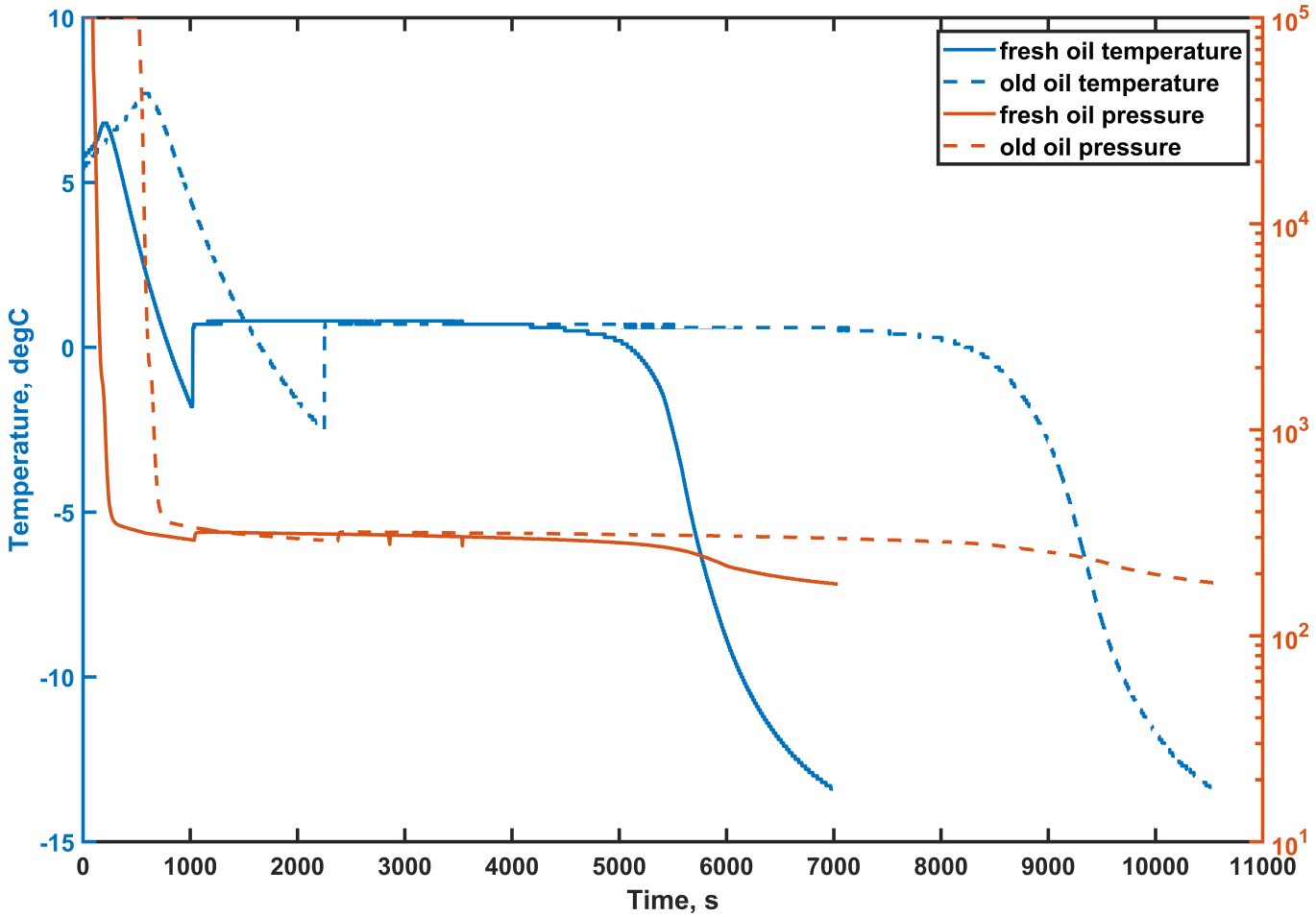

Figure 4.1.5: Temperature and pressure profiles of vacuum freezing of water RS sponge in two separate tests with used and fresh oil

of the process, and then was slightly closed to reduce the pressure to 250 Pa for the rest of the vacuum freezing. In second run, valve was completely shut, and pressure was set to 10 Pa. This resulted in quite significant difference in pressure between two performed tests. In result, temperature drop in both cases was very similar, but the freezing plateau was 500 seconds shorter in the process with closed valve, which resulted in 500 seconds temperature "lag" between two cases, meaning, that the time of reaching -5 °C, -10 °C, -20 °C and so on, was different by 500 seconds.

4.1.6 Influence of refrigeration system

The lowest achievable pressure depends on rate of evaporation, pumping speed, and leakage. The latter is the most observable at very low pressures, where pressure reduction rate drops drastically due to the pump characteristic. During tests, it was discovered that temperature of the refrigerant has a crucial influence on the low pressure limit. Since evaporating vapour is resublimating at the outer walls of the coil filled with refrigerant, the partial pressure of the now resublimated ice is equal to saturation pressure corresponding to temperature of the coils outer wall. For example, if temperature of the wall is equal to -10 °, the partial pressure of gas above the ice is approximately equal to 260 Pa. If the wall temperature would be just 10 °C lower, the partial pressure would now be around

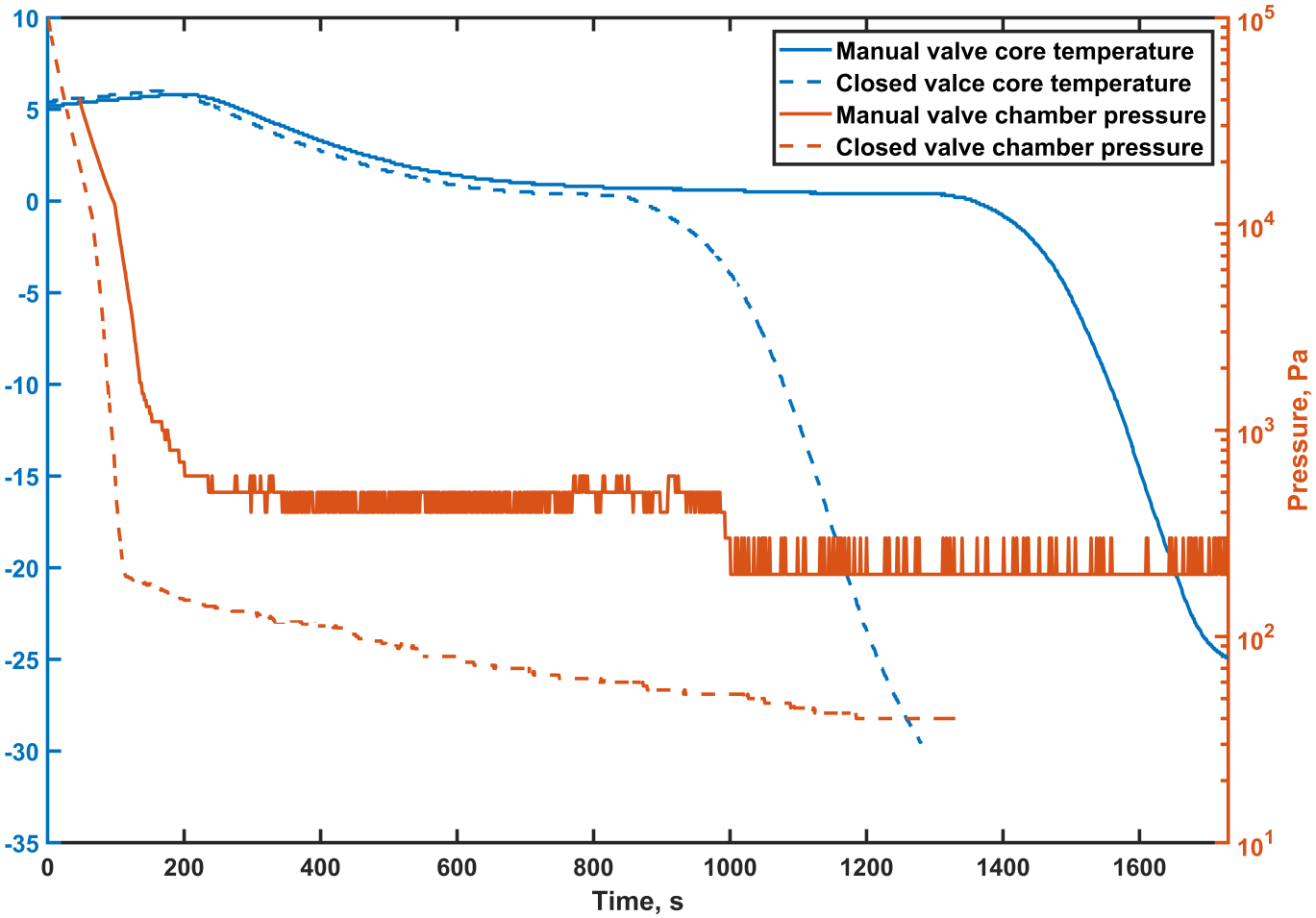

Figure 4.1.6: Temperature and pressure profiles of vacuum freezing of water RS sponge in two separate tests with closed and open pressure valve

103 Pa. The temperature-pressure relation is shown at Fig. .0.4 and is a matter of a compromise - lower temperature results in lower pressure, but at some point reduction of temperature reduces the saturation pressure by barely noticeable values. The cost of cooling the refrigerant also increases drastically the lower the temperature is desired. It must be noted, that reducing the pressure of the system below saturation pressure of the refrigerant temperature will result in no resublimation of the vapour at the coil, thus making the whole evaporator useless, since all of the evaporated moisture will be evacuated directly into the pump, which effectiveness will be reduced, and eventually the pump will get damaged.

4.1.7 Mass loss

The difference in mass loss to temperature drop ratio between the two devices, namely 22.4% in µWaveVac0250 and 15.6% in LyoCube is caused by the lack of cooling unit in LyoCube. The energy released by the nucleation caused by supercooling results in sudden increase in temperature and greatly reduces further temperature drop rate. During this time vapour is evaporating and sublimating from the sponge, reducing the mass of the sample, without decrease of temperature.

4.1.8 Initial freezing point

At first, the initial freezing point was assumed to be the one of water, 0 °C or up to a -1 °C below due to both contamination in form of minerals, and influence of porous sponge in which the water is stored. But according to Fig. 4.1.3, plateau occurring after nucleation in the experiments, the actual initial freezing temperature is indicated to be approximately 0.4 °C.

4.2 Experimental vacuum freezing of the potato slice

4.2.1 Temperature

Fig. 4.2.1 and Fig. 4.2.2 show the pressure and temperature profiles of the process, with the first one showing averaged results of 3 tests of separate samples with standard deviations, and the latter displaying results of each individual sample. On average, in cooling stage, cooling rate was equal to 1.26 °C/minute, and began to decelerate when approaching the initial freezing temperature of -1.6 °C, and when the temperature was in the range from to -3 °C to -4 °C, the supercooling occurred, after which the temperature of potato was being reduced at a rate of 0.07 °C/minute. The highest temperature difference between the core and the surface of the potato can be seen in the cooling stage, and is equal up to 3.5 °C. That temperature difference is naturally caused by the quicker start of moisture evaporation process in the surface of the product, opposed to the core, caused by the permeability of the media which prevents the partial pressure in the core to be reduced as fast as in the surface. As can be seen in Fig. **??**, in the freezing stage, on average the difference in temperature between measured points was lower than in the second stage, and was equal to up to 1.2 °C. Fig. **??** shows that in test T1 the difference was higher, up to 3 °C, but in sample T3 the difference was equal to 1.6 °C, and in sample T2 it was lower than 1 °C. About an hour after the supercooling, the temperatures in the core and in the surface equalized, and difference was equal to approx. 0.3 °C.

Table 4.2.1: Standard deviations of temperature during the vacuum freezing of potato slices

Measured point	Average $\frac{dT}{d\tau}$	Average STD	Initial STD	End STD
Core	0.0033	0.68	0.76	0.49
Surface	0.0032	1.51	0.79	0.7

4.2.2 Pressure

The pressure in the chamber got to the saturation pressure equal to 2350 Pa of initial sample temperature of 20 °C in approximately 166 seconds. Before that, slight reduction of temperature was observed in the surface, most likely due to the lower air pressure in the chamber. Finally, the pressure reached approx. 300 Pa. during the phase change process. Due to the intensive evaporation, leakage and vacuum pump characteristics the further decrease of the vacuum pressure was relatively slow. In the end of the process, the pressure was equal to 223Pa, and time between reaching 300 Pa and 223 Pa was 117 minutes, which is high compared with required 13 minutes to reach 300 Pa from 101325 Pa.

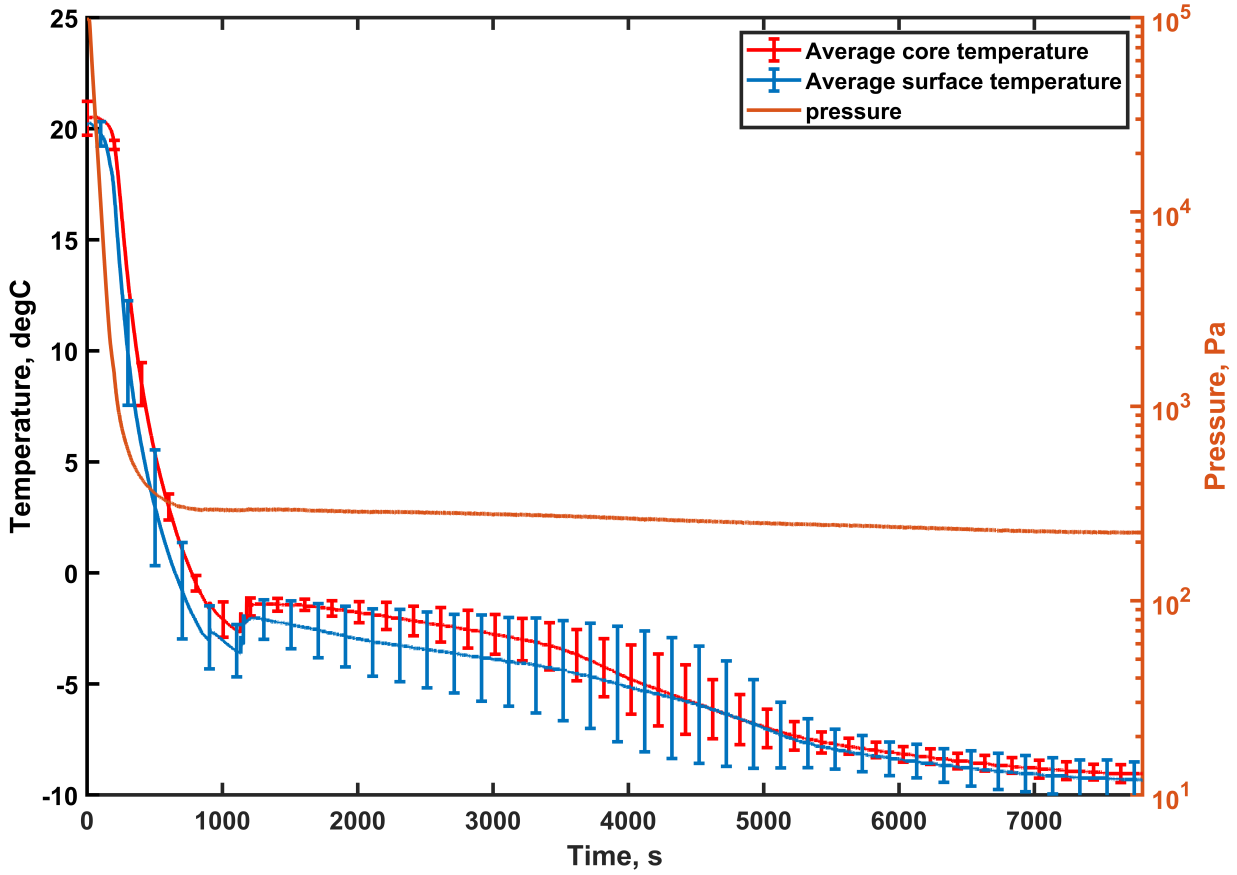

Figure 4.2.1: Averaged temperature profiles of vacuum freezing of potato slice

4.2.3 Supercooling and plateau

Due to the energy released with supercooling, the temperature rose by randomly from 1 °C and up to 4 °C, depending on particular slice. The increase of temperature of a specific potato slice was completely random. The nucleation happened either instantly in both measured points, or was delayed by up to 25 seconds in the core. Sometimes the temperature in the surface increased more than the core and on different occasions the temperature of two measured points increased by equal value. One must be noted, that the temperature of the surface never rose above the temperature of the core. The plateau was almost unnoticeable in certain slices, and in different ones could take up to 50 minutes. This is certainly caused by the random character of occurring of supercooling, the impossible to avoid small differences in composition of each slice, and the accuracy of the exact placement of thermocouple.

4.2.4 Mass loss

Potatoes were measured in bulk before and after the process, giving the information about the overall mass loss during the whole process. On average, the mass loss was equal to 23% during the 132 minute vacuum freezing process where temperature dropped by 29.5 °C.

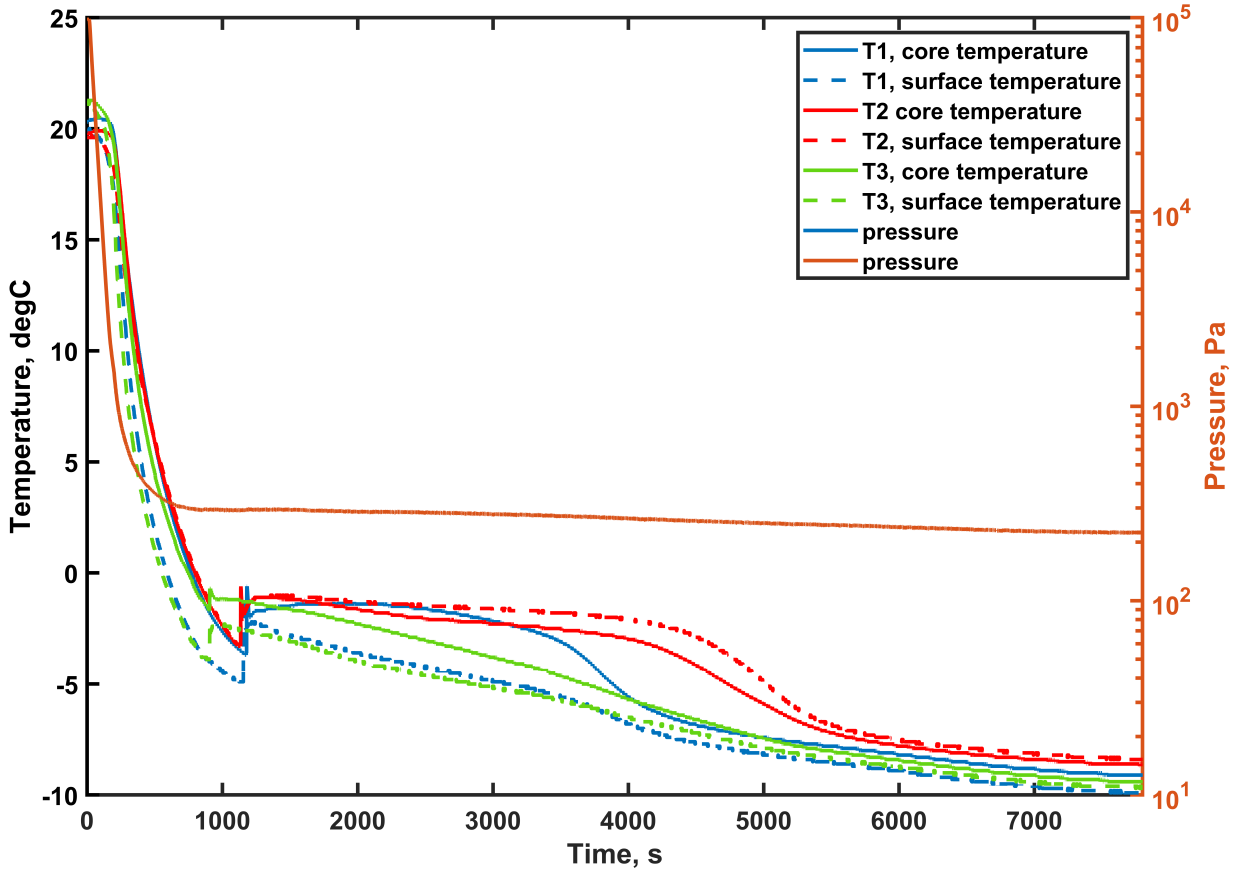

Figure 4.2.2: Temperature profiles of vacuum freezing of 3 separate potato slices

4.2.5 Initial freezing point

The freezing point was observed to be about -1.6 °C.

4.2.6 Cooling system

The temperature of the refrigerant during the whole process was in the range of -32 °C to -30°C in the inlet of evaporator coil, and -15 °C to -23 °C in the outlet.

4.3 CFD model validation

Preliminary CFD model was validated based on experimental data from vacuum freezing tests of RS sponge and vacuum freezing tests of potato slice.

4.3.1 RS sponge CFD model validation

The validation of RS sponge experiments. Since the nucleation and temperature plateau didn't occur in the experiments of vacuum freezing of water RS sponge in µWaveVac0250, for this specific case the CFD model excluded the Chen's approach for the specific heat and enthalpy that simulates the temperature plateau of nucleation. In that case, the

model does not the into the account the latent heat of phase change of liquid water into ice when calculating the specific heat and enthalpy. In effect, no temperature plateau is occurring around the temperature range of initial freezing point. The sudden but very short increase of temperature reduction rate that can be visible after the local temperature drops below the initial freezing point is caused by the difference in specific heat of ice and water, with the value of the latter being almost twice as high. The accuracy of the temperature profiles between the experimental results and preliminary CFD model is not ideal. In the cooling stage the discrepancy is quite low, but it increases in the freezing stage. It is very highly probable, that in later part of the process the changes in material properties as well as changes in the saturation of phases. The apparent shrinkage of the material is not taken into the account in the preliminary model, and could have an impact on the temperature profiles. The specific material properties of RS sponge and its changes during the process might be the reason for inaccuracy of the model, especially in later stage of the simulation.

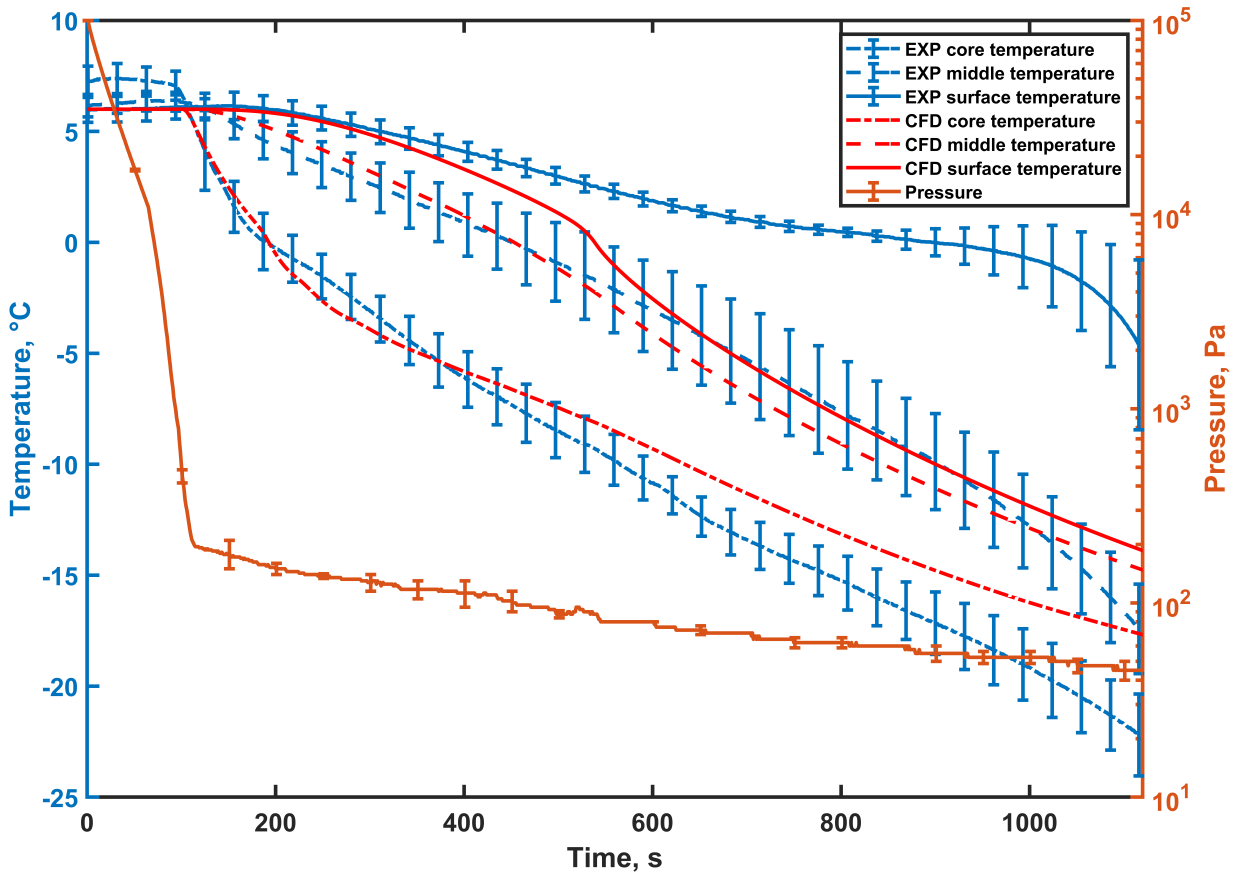

Figure 4.3.1: CFD model validation for vacuum freezing of water RS sponge in µWaveVac0250 device

4.3.2 Potato CFD model validation

Compared to validation of RS sponge experiments, validation of potato tests proved to be much more accurate, which can be explained by the smaller length between measured

points, due to the potato slice being significantly smaller than the analysed RS sponge. The lower discrepancy can also be caused by the structure of the potato being more firm and denser than the RS sponge.

In the cooling stage, the CFD temperature profiles are a bit higher than in the experiments, most likely due to the fact, that the potato sample in the chamber during the experiments started to cool down before the chamber pressure reached saturation pressure. Time of nucleation occurrence and the duration of temperature plateau is in good agreement between the validation and experiment. The simulated temperature is higher than in the experiment until the 95 minute mark, where the rate of temperature decrease in CFD case is faster than in the experiment, and the CFD model shows lower temperatures. At the end of the simulated process the surface and core of the potato have the same temperature, and the difference between simulated temperature, and the experimental data is 2 °C.

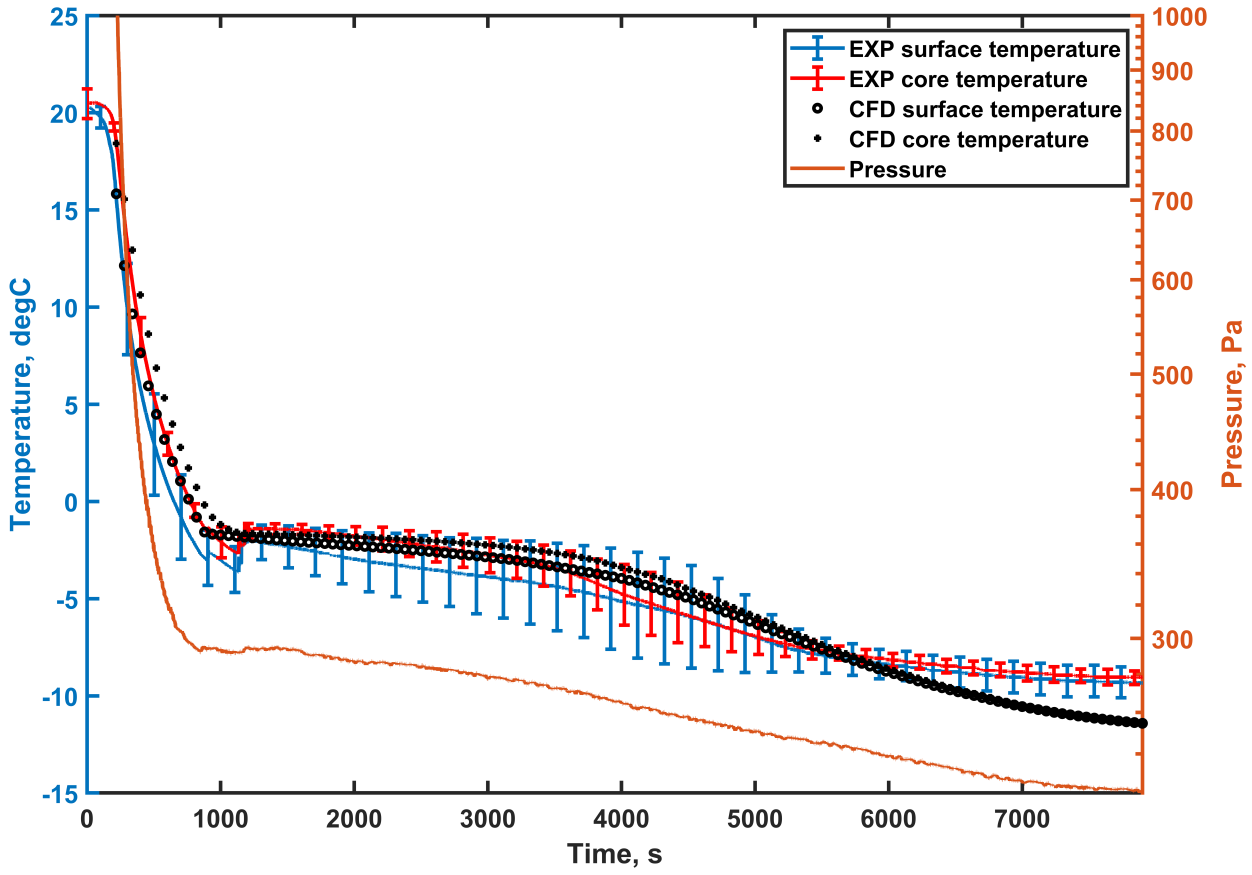

Figure 4.3.2: CFD model validation for vacuum freezing of potato slice

4.4 Sensitivity analysis

To analyse the impact of the absent, very brief or impossible to document parameters on the model, sensitivity analysis was performed. Evaporation constant K_{evap}, porosity of the potato ϕ, intrinsic permeability of gas α_g and initial volume fraction of vapour φ were

analysed in terms of its impact on the temperature profiles. The porosity has cosmetic influence on the process, with lower values increasing the temperature reduction rate. The vapour intrinsic permeability and vapour fraction has a gigantic influence on the process. The first one dictates the rate at which the built-up pressure from evaporation can leave the domain. The higher the intrinsic permeability, the faster the pressure can leave through the boundary, thus increasing the difference between partial pressure and saturation pressure of water, which is the driving force of the vacuum freezing process. Low permeability causes the partial pressure in the inside of the product to accumulate, causing the partial pressure to be higher than saturation temperature, and prohibiting the local evaporation. Apart from the thermal conductivity, this property can be fitted to control the temperature difference along a specific length. The impact of the vapour fraction on the other hand is caused by the large difference of thermal and physical properties between phases present in the pores. As pores must be occupied by either water vapour-air mixture, or liquid water, the higher initial volume fraction of the first one causes the reduction of the latter. More importantly, the values of thermal conductivity, specific heat, density, etc. are much lower for gas mixture than for the liquid water.

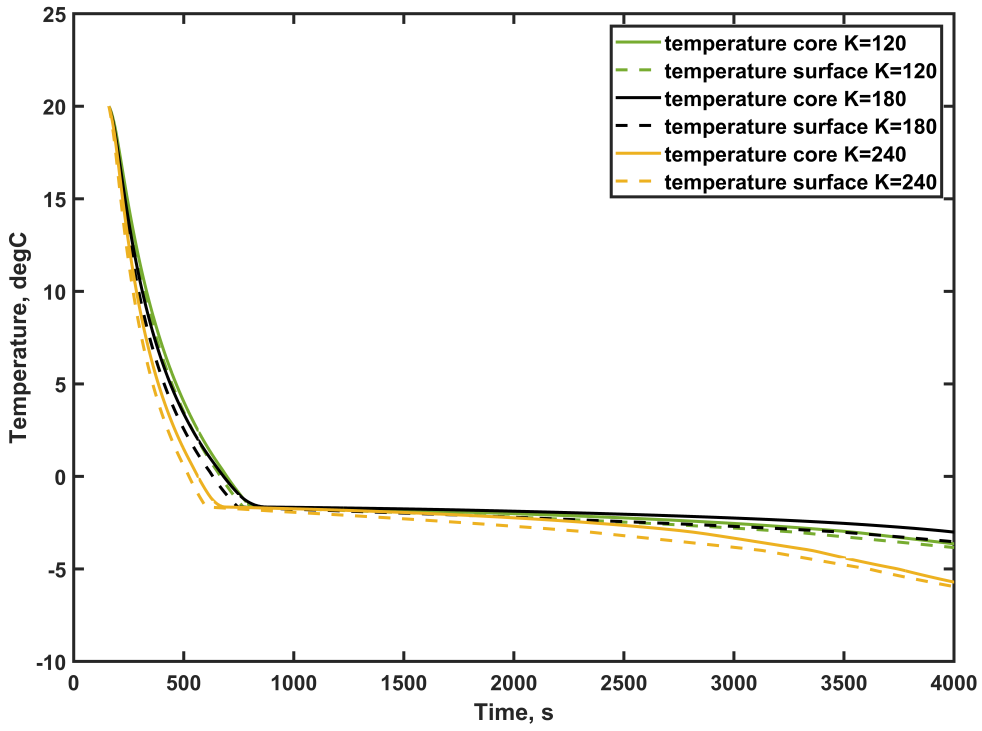

Figure 4.4.1: Sensitivity analysis of evaporation constant in potato case

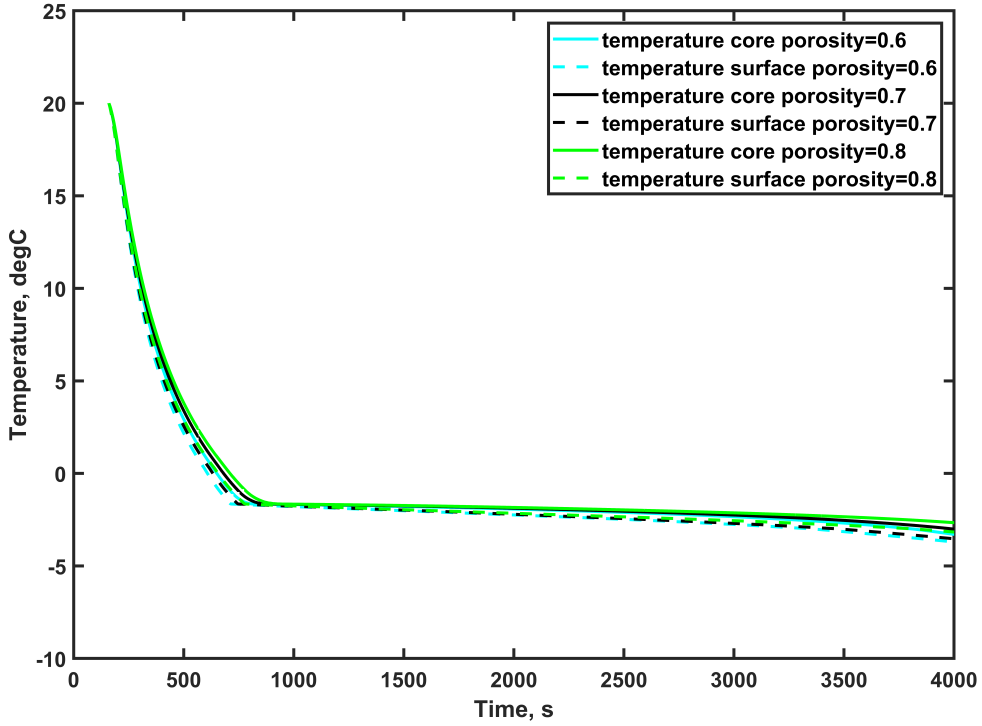

Figure 4.4.2: Sensitivity analysis of porosity in potato case

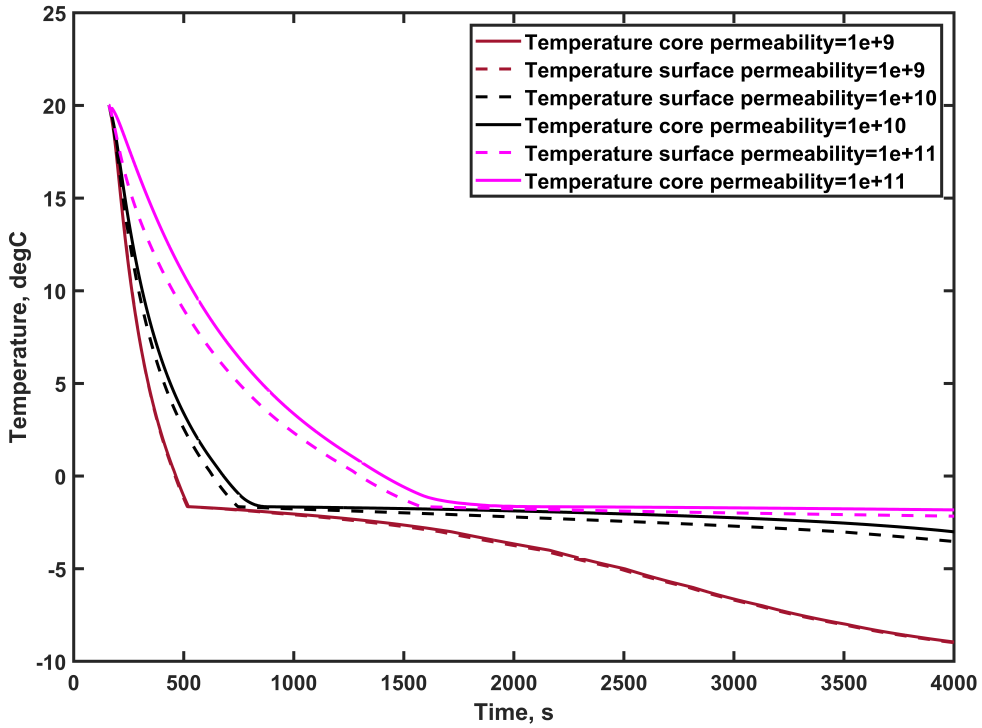

Figure 4.4.3: Sensitivity analysis of intrinsic permeability of gas in potato case

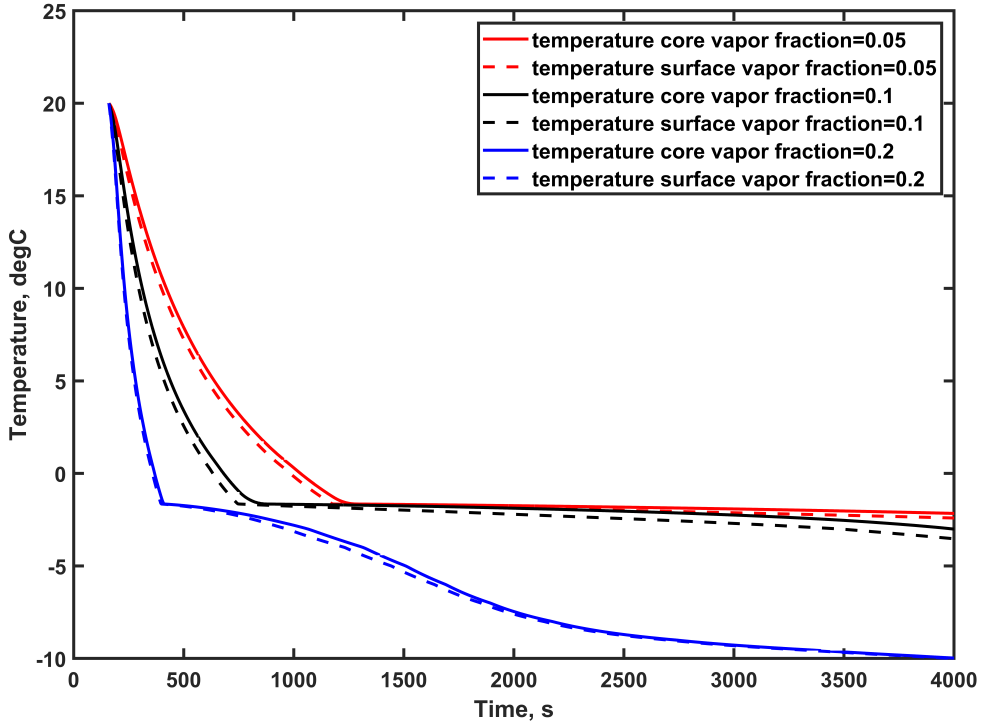

Figure 4.4.4: Sensitivity analysis of initial vapour volume fraction in potato case

CHAPTER
FIVE

CONCLUSIONS

5.1 Vacuum freezing process

Vacuum freezing technique allows for cooling and freezing in a rapid rate, and for certain foods such as fruits [31], vegetables [59] much quicker than conventional methods. The evaporative character of this method allows to reduce the moisture content of food, thus making it less probable for bacteria and contamination to occur during the time of transportation and reducing the overall food loss in the cold-chain. With less moisture content, shelf life of vacuum freezed products is higher when compared with other methods, further reducing the food loss and food waste.

5.2 Parameters of the vacuum freezing system

5.2.1 Pressure

Investigation of vacuum freezing process using µWaveVac0250 machinery with different pressure reduction rate was conducted. The results indicate a great influence of the chamber pressure on the time required for a core of the product to reach desired temperature. Additionally, when comparing the results achieved in µWaveVac0250 which has a lower pressure limit, at which the pressure reduction rate suddenly decreases due to the pump characteristic, cooling capacity of freezing system, and leakage, around 100 Pa, and those in LyoCube which lower pressure limit is equal to 300 Pa, the difference in time of the process is very clear, and the vacuum freezing process in µWaveVac0250 is about 5-10 times faster, which is in big part caused by the pressure reduction rate and a pressure lower limit.

5.2.2 Cooling system

Based on enormous difference of the temperature profiles and time of vacuum freezing process between LyoCube and µWaveVac0250 experiments, the assumption can be made, that the cooling system has a significant effect on the time and effectiveness of vacuum freezing process. Not only does it reduce the lower pressure limit by condensing the evaporating water vapour on the evaporator's coil thus reducing the chamber pressure, but also is crucial for preventing the degradation of vacuum pump and oil, which was proven

in Section 4.1.3. However, the experiments in the VacPCM stand, which was equipped with cooling system as well as the µWaveVac0250 machinery, show that the temperature plateau due to the nucleation still occurred. Based on that, it may be assumed that the temperature plateau due to the release of latent heat of certain products that have a similar material composition as the water RS sponge may be omitted by the use of cooling system.

5.3 Numerical model of vacuum freezing process

A few models simulating vacuum cooling are available in the literature and publications [31, 32, 33, 34, 35, 36, 37], but so far no detailed vacuum freezing model have been developed, with an exception of a vacuum freezing model of a single 1-D droplet [38, 39]. Addition of phase change and freezing to a vacuum cooling model is a novelty and could be a break through in simulating freezing process in vacuum freezers. Developed preliminary 3-D numerical CFD model is a big step in advancement of vacuum freezing simulations, even if the results are not in great agreement with experimental data.

The developed numerical model allows for simulating vacuum freezing process of foods. Due to the used mathematical equations, model can be used for a variety of food products based on their composition. Two simulations were presented, one accounting the vacuum freezing of the RS sponge, and the second model relating to the vacuum freezing of potato slice. The accuracy of the temperature profiles of water in RS sponge model leaves much to be desired, mostly due to the large size of the sample, prone to the internal heat resistance. Also the specific properties of the sponge material can cause heat leakage, water spillage, and substantial shrinkage of the material followed by the appearance of holes around the temperature measuring probes. Additionally, the discrepancy of the temperature profiles between µWaveVac0250 simulation and experimental data is increased due to the extremely high pressure reduction and cooling rate. Due to the enormous size of the µWaveVac0250 cooling system and heat capacity of the condenser, supercooling phenomenon did not occur during the process. On the other hand, the validation of the potato slices experiments showed favourable results. The achieved accuracy of the temperature profiles is satisfactory. Compared to the less accurate validation of the water in RS sponge, it is safe to say that the smaller size of the sample as well as more unified and denser structure of the sample is the reason for the better accuracy of the potato validation. Nucleation and supercooling proved to be a challenge to model correctly, due to the randomness of said phenomena, so the accuracy of temperature profile during the supercooling stage is lower when compared to the rest of the process. Nonetheless, the presented approach of increasing the specific heat of a product and omitting the supercooling effect of temperature dropping below initial freezing temperature simulates well the freezing plateau. Conducted sensitivity analysis showed that the parameters which values are unavailable, undocumented or hard to estimate, have enormous impact on the simulation results. Results of an experimental estimation of such parameters will differ greatly between foods and even batches of same foods, meaning the the experimental assessment will most likely need to be performed specifically for the purpose of modelling.

5.4 Applicability of the CFD model

Based on the agreement of CFD validation results and data from vacuum freezing of potatoes, the model could be applied to perform optimisation, general performance tests of vacuum freezing process by changing the pumping speed which affects the pressure, different placement or preparation of load, which affects the evaporation rate due to different effective surface. The above parameters are one of many factors that need to be carefully set to reduce the energy demand of the plant, while remaining the effectiveness. Usage of the model beforehand could be a cheaper alternative to eliminate certain solutions.

5.5 Evaluation of impact on the cold-chain

Vacuum freezing technique allows for cooling and freezing in a rapid rate, and for certain foods much quicker than conventional methods. Foods with high moisture and high surface to volume ratio, such as certain fruits [31], vegetables [59, **?**] or meats [60], can benefit the most from the vacuum freezing method of freezing. The evaporative character of this method allows to reduce the moisture content of food, thus making it less probable for bacteria and contamination to occur during the time of transportation and reducing the overall food loss in the cold-chain. With less moisture content, shelf life of vacuum freezed products is higher when compared with other methods, further reducing the food loss and food waste. The above factors could improve the efficiency, integrity and sustainability of foods in cold chain and cold chain itself. Introducing vacuum freezing method to cold chain could help reduce the duration of precooling stage of cold chain, while possibly reducing its operational cost.

5.6 Future work

The selection of RS sponge filled with water as a analysed sample was caused by the unavailability of meaningful food properties, as well as its difference between each tested sample. The difference between validation of potato slice and water RS sponge proves that the CFD model in its current state is not suitable for all products, and the integrity of the CFD model as well as mathematical equations and solver settings should be thoroughly verified. For the increase of model's availability and accuracy, future validation should be conducted based on experimental data regarding vacuum freezing of a broader variety of food products. To achieve better accuracy of the model, partial pressure of the food's moisture should be taken into consideration when estimating the thermal and physical properties of the material. It's effect on the properties was omitted duo to the no availability of experimental data that correlates the effect of both the pressure and temperature on product's properties. Besides, in the future experimental tests, the samples must be stored in an environment in which the temperature is the same as the temperature in the chamber. That action will eliminate the temperature discrepancy between each sample, and within the sample itself, resulting in higher fidelity of each individual test. That would also reduce the uncertainty of CFD model results. Most importantly, permeability, porosity and initial volume fraction of air of certain foods should be investigated to at least narrow the possible range of those values, which have a substantial impact on the results of the presented CFD model. The model should also be improved in

terms of solver schemes, to better simulate the concentration of moisture and gas in the domain, which could influence the accuracy of the model due to the very different thermal properties of the gas and liquid phases. Additionally, the shrinkage of the material should be taken into consideration, which would allow for eliminating the high imbalance in mass loss results of the CFD model and experimental data. Furthermore, parametric analysis of influence of process parameters such as pressure, refrigerant temperature should be performed to ensure the good approximation of pressure-evaporation rate.

BIBLIOGRAPHY

[1] Pfeiffer okta500 pump characteristic. https://www.pfeiffer-vacuum.com/en/products/vacuum-generation/roots-pumps/universal-boosters/oktaline/okta-500/3216/okta-500-roots-vacuum-pump-230-400-v-50-hz-265-460-v-60-hz.

[2] Pfeiffer duo65 pump characteristic. https://www.pfeiffer-vacuum.com/en/products/vacuum-generation/rotary-vane-pumps/two-stage/standard/30897/duo-65-rotary-vane-pump-220-380-v-60-hz-3tf.

[3] Edwards 12rv12 vacuum pump characteristic. https://www.edvac.pl/upload/2020/10/file-23.pdf.

[4] Wikimedia Commons. Phase diagram of water, 2023. [Online; accessed 31-August-2023].

[5] Characteristics of rs sponge.

[6] Kelvin O. Yoro and Michael O. Daramola. Chapter 1 - CO2 emission sources, greenhouse gases, and the global warming effect. In Mohammad Reza Rahimpour, Mohammad Farsi, and Mohammad Amin Makarem, editors, *Advances in Carbon Capture*, pages 3–28. Woodhead Publishing, 2020.

[7] Nadine Borduas and Neil M. Donahue. Chapter 3.1 - the natural atmosphere. In Béla Török and Timothy Dransfield, editors, *Green Chemistry*, pages 131–150. Elsevier, 2018.

[8] The evidence is clear: the time for action is now. We can halve emissions by 2030. — IPCC.

[9] Co2 emissions in 2022.

[10] Energy is at the heart of the solution to the climate challenge — IPCC.

[11] IPCC. *Climate Change 2022: Impacts, Adaptation and Vulnerability*. Summary for Policymakers. Cambridge University Press, Cambridge, UK and New York, USA, 2022.

[12] G.F. Hundy, A.R. Trott, and T.C. Welch. Chapter 17 - the cold chain – transport, storage, retail. In G.F. Hundy, A.R. Trott, and T.C. Welch, editors, *Refrigeration, Air Conditioning and Heat Pumps (Fifth Edition)*, pages 273–287. Butterworth-Heinemann, fifth edition edition, 2016.

[13] Jia-Wei Han, Min Zuo, Wen-Ying Zhu, Jin-Hua Zuo, En-Li Lü, and Xin-Ting Yang. A comprehensive review of cold chain logistics for fresh agricultural products: Current status, challenges, and future trends. *Trends in Food Science & Technology*, 109:536–551, March 2021.

[14] https://www.un.org/en/observances/end-food-waste-day.

[15] The state of food and agriculture 2019. moving forward on food loss and waste reduction.

[16] United Nations Environment Programme. Food waste index report 2021, 2021.

[17] FAO. Tackling food loss and waste: A triple win opportunity, 2022.

[18] Shukrullah Sherzad. Post-harvest losses along value and supply chains in the pacific island countries. 06 2015.

[19] World Health Organization. Food safety. Technical report.

[20] Karl Mcdonald and Da-Wen Sun. Vacuum cooling technology for the food processing industry: a review. Technical report.

[21] Ding Tian, Liu Fen, Ling Jiangang, Kang Mengli, Yu Jingfen, Ye Xingqian, and Liu DongHong. Comparison of different cooling methods for extending shelf life of postharvest broccoli. *Biol Eng*, 9, 2016.

[22] Zhiwei Zhu, Yi Geng, and Da-Wen Sun. Effects of operation processes and conditions on enhancing performances of vacuum cooling of foods: A review. *Trends in Food Science & Technology*, 85:67–77, March 2019.

[23] S. Y. He, G. P. Feng, H. S. Yang, Y. Wu, and Y. F. Li. Effects of pressure reduction rate on quality and ultrastructure of iceberg lettuce after vacuum cooling and storage. *Postharvest Biology and Technology*, 33(3):263–273, September 2004.

[24] Tingting Qi, Jun Ji, Xuelai Zhang, Lu Liu, Xinhong Xu, Kunlin Ma, and Yintao Gao. Research progress of cold chain transport technology for storage fruits and vegetables. *Journal of Energy Storage*, 56:105958, 2022.

[25] Patrick Dempsey and Pradeep Bansal. The art of air blast freezing: Design and efficiency considerations. *Applied Thermal Engineering*, 41:71–83, 2012. 13th Brazilian Congress of Thermal Sciences and Engineering.

[26] Air blast freezers. `http://ecoursesonline.iasri.res.in/mod/page/view.php?id=3453`.

[27] Fao, intruduction to freezing. `https://www.fao.org/3/y5979e/y5979e03.htm`.

[28] Dongwu Liang, Fengying Lin, Gongming Yang, Xiju Yue, Quankai Zhang, Zhaoqi Zhang, and Houbin Chen. Advantages of immersion freezing for quality preservation of litchi fruit during frozen storage. *LWT - Food Science and Technology*, 60(2, Part 1):948–956, 2015.

[29] Chapter 7.1 - refrigeration. In Rémy Cachon, Philippe Girardon, and Andrée Voilley, editors, *Gases in Agro-Food Processes*, pages 223–318. Academic Press, 2019.

[30] Caihu Liao and Yigang Yu. Effect of vacuum cooling followed by ozone repressurization on Clostridium perfringens germination and outgrowth in cooked pork meat under temperature-abuse conditions. *Innovative Food Science & Emerging Technologies*, 68:102599, March 2021.

[31] Bin Dai, Ankang Kan, and Bo Yi. An improved mathematical model bidirectional coupling of heat-water and mechanics during vacuum pre-cooling. *Innovative Food Science and Emerging Technologies*, 81, October 2022. Publisher: Elsevier Ltd.

[32] T. X. Jin and L. Xu. Development and validation of moisture movement model for vacuum cooling of cooked meat. *Journal of Food Engineering*, 75(3):333–339, August 2006.

[33] Xiao Yan Song, Bao Lin Liu, and Ganesh K. Jaganathan. Mathematical simulation on the surface temperature variation of fresh-cut leafy vegetable during vacuum cooling. *International Journal of Refrigeration*, 65:228–237, May 2016. Publisher: Elsevier Ltd.

[34] Alexander Warning, Ashim K. Datta, and Jerry A. Bartz. Mechanistic understanding of temperature-driven water and bacterial infiltration during hydrocooling of fresh produce. *Postharvest Biology and Technology*, 118:159–174, August 2016. Publisher: Elsevier B.V.

[35] Zipei Huang, Ankang Kan, Jiaxi Lu, Fuliang Li, and Tongzhou Wang. Numerical simulation and experimental study of heat and mass transfer in cylinder-like vegetables during vacuum cooling. *Innovative Food Science & Emerging Technologies*, 68:102607, March 2021.

[36] T. X. Jin and L. Xu. Numerical study on the performance of vacuum cooler and evaporation-boiling phenomena during vacuum cooling of cooked meat. *Energy Conversion and Management*, 47(13-14):1830–1842, August 2006.

[37] Mohsen Ranjbaran and Ashim K. Datta. Pressure-driven infiltration of water and bacteria into plant leaves during vacuum cooling: A mechanistic model. *Journal of Food Engineering*, 246:209–223, April 2019. Publisher: Elsevier Ltd.

[38] Zhijun Zhang, Jingxin Gao, and Shiwei Zhang. Heat and Mass Transfer of the Droplet Vacuum Freezing Process Based on the Diffusion-controlled Evaporation and Phase Transition Mechanism. *Scientific Reports*, 6, October 2016. Publisher: Nature Publishing Group.

[39] C. Cogné, P. U. Nguyen, J. L. Lanoisellé, E. Van Hecke, and D. Clausse. Modeling heat and mass transfer during vacuum freezing of puree droplet. *International Journal of Refrigeration*, 36(4):1319–1326, June 2013.

[40] Hans Pruppacher, James Klett, and Pao Wang. Microphysics of clouds and precipitation. *Aerosol Science and Technology*, 28:381–382, 01 1998.

[41] D. Duft and T. Leisner. Laboratory evidence for volume-dominated nucleation of ice in supercooled water microdroplets. *Atmospheric Chemistry and Physics*, 4(7):1997–2000, 2004.

[42] Richard P. Sear. Quantitative studies of crystal nucleation at constant supersaturation: experimental data and models. *CrystEngComm*, 16:6506–6522, 2014.

[43] Q. Tuan Pham. *Food Freezing and Thawing Calculations*. Springer New York, NY, 2104.

[44] C S Chen. Thermodynamic Analysis of the Freezing and Thawing of Foods: Enthalpy and Apparent Specific Heat. Technical report.

[45] James K. Carson, Jianfeng Wang, Mike F. North, and Donald J. Cleland. Effective thermal conductivity prediction of foods using composition and temperature data. *Journal of Food Engineering*, 175:65–73, April 2016. Publisher: Elsevier Ltd.

[46] F.L Levy. A modified maxwell-eucken equation for calculating the thermal conductivity of two-component solutions or mixtures. *International Journal of Refrigeration*, 4(4):223–225, 1981.

[47] G. Tchiegeov. Thermophysical processes in food refrigeration technology. *Food industry*, 1979.

[48] H. Feng, J. Tang, O.A. Plumb, and R.P. Cavalieri. Intrinsic and relative permeability for flow of humid air in unsaturated apple tissues. *Journal of Food Engineering*, 62(2):185–192, April 2004.

[49] Donald A. Nield and Adrian Bejan. *Convection in Porous Media*. Springer, New York, NY, 2013.

[50] Wavevac datasheet. `https://www.pueschner.com/downloads/vacuumdrying.pdf`.

[51] Huber unistat 905 datasheet. `http://www.huber-usa.com/download/pdf_datasheets/englisch/1054.0007.01.PDF`.

[52] Lyocube 4-8 lsc datasheet. `https://yiqi-oss.oss-cn-hangzhou.aliyuncs.com/aliyun/900100631/technical_file/file_177419.pdf`.

[53] Edwards 12 rv12 rotary vane vacuum pump datasheet. `https://www.ajvs.com/library/Edwards_RV_Series_Brochure.pdf`.

[54] Ansys fluent 12.0 user's guide.

[55] A. Halder, A. Dhall, and A. K. Datta. An improved, easily implementable, porous media based model for deep-fat frying. Part I: Model development and input parameters. *Food and Bioproducts Processing*, 85(3 C):209–219, 2007. Publisher: Institution of Chemical Engineers.

[56] Michal Stebel, Jacek Smolka, Michal Palacz, Edyta Piechnik, Michal Halski, Magdalena Knap, Ewa Felis, Trygve Magne Eikevik, Ignat Tolstorebrov, Juan Manuel Peralta, and Susana E. Zorrilla. Numerical modelling of the food freezing process in a quasi-hydrofluidisation system. *Innovative Food Science and Emerging Technologies*, 74, December 2021. Publisher: Elsevier Ltd.

[57] M Shafiur Rahman. Food Properties Handbook Second Edition. Technical report.

[58] Warren L. (Warren Lee) McCabe, 1899-1982. *Unit operations of chemical engineering.* Sixth edition. Boston : McGraw Hill, [2001] ©2001, 2001.

[59] Zhiwei Zhu, Xinwei Wu, Yi Geng, Da-Wen Sun, Haiyang Chen, Yongjun Zhao, Wenqing Zhou, Xianguang Li, and Hongzhun Pan. Effects of modified atmosphere vacuum cooling (MAVC) on the quality of three different leafy cabbages. *LWT*, 94:190–197, August 2018.

[60] Lijun Wang and Da-Wen Sun. Modelling vacuum cooling process of cooked meat-part 2: mass and heat transfer of cooked meat under vacuum pressure. Technical report.

APPENDICES

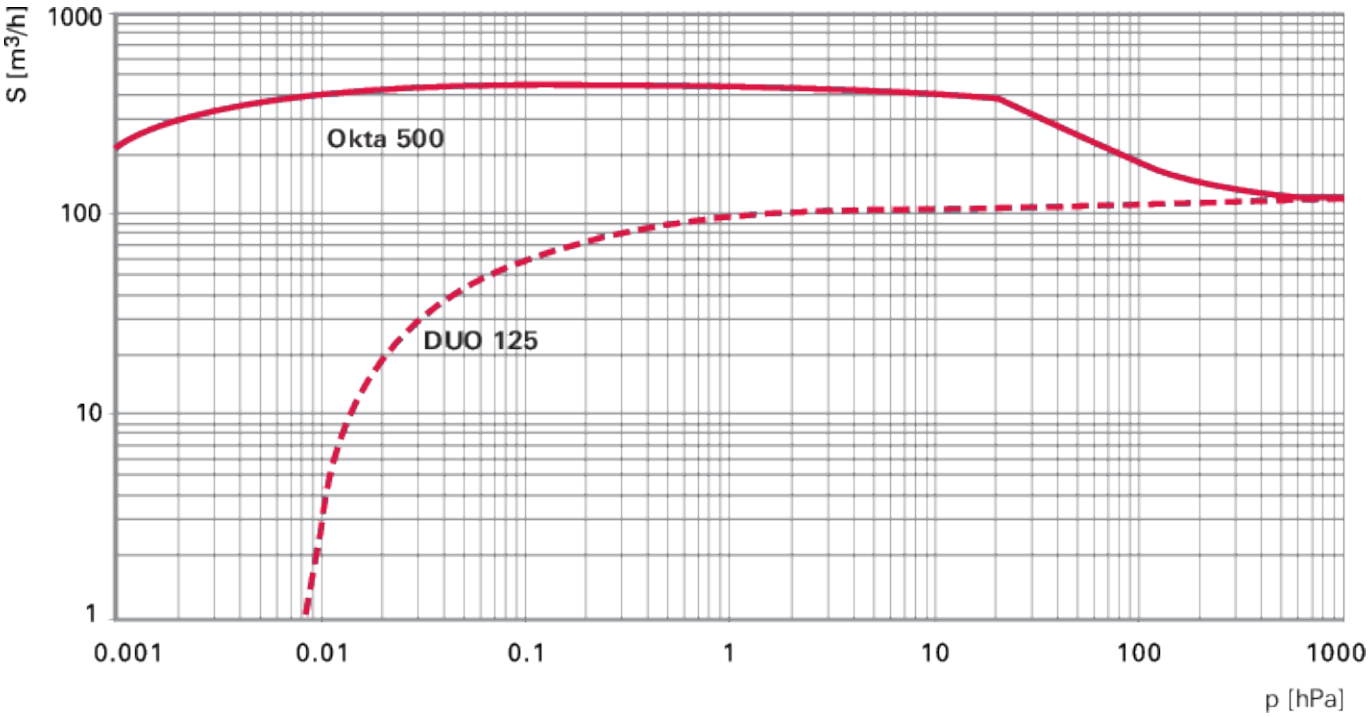

Figure .0.1: Characteristic of Pfeiffer Okta 500 vacuum pump [1]

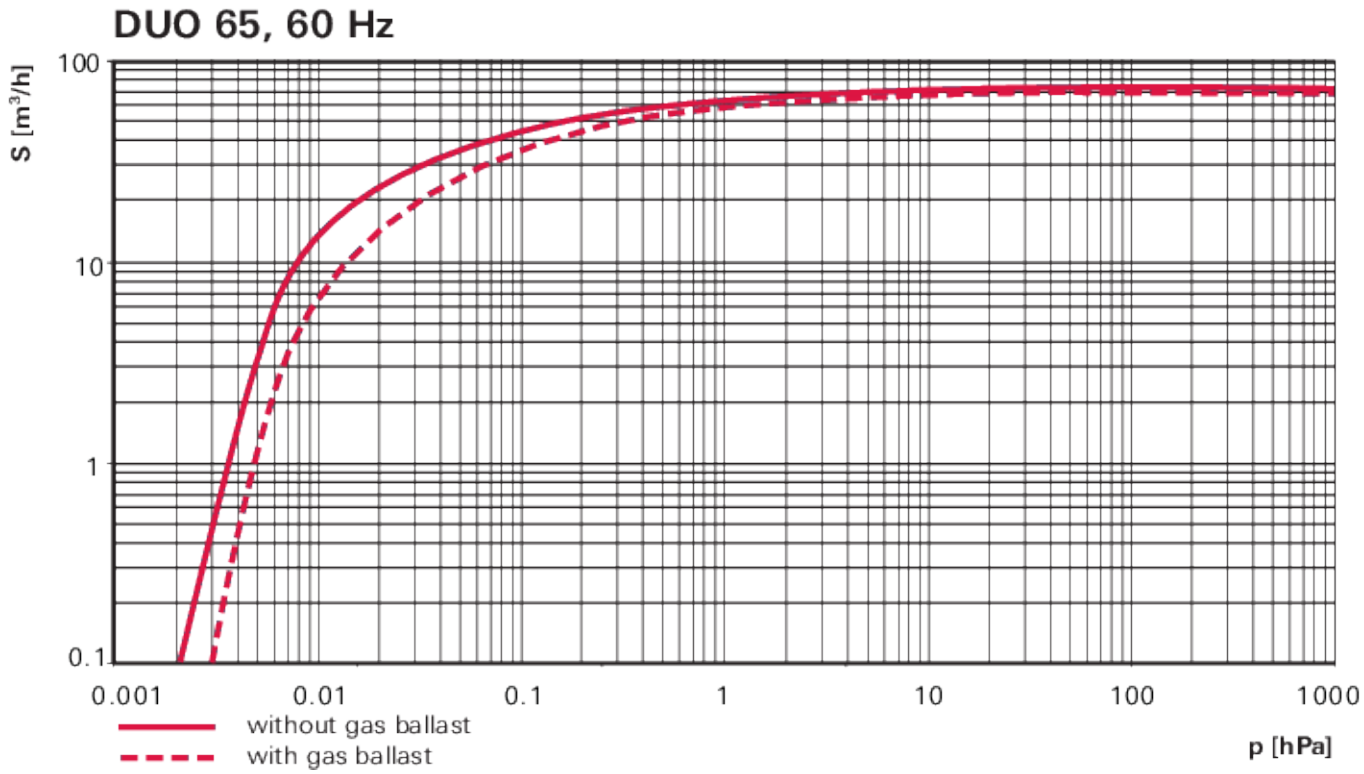

Figure .0.2: Characteristic of Pfeiffer DUO 65 vacuum pump [2]

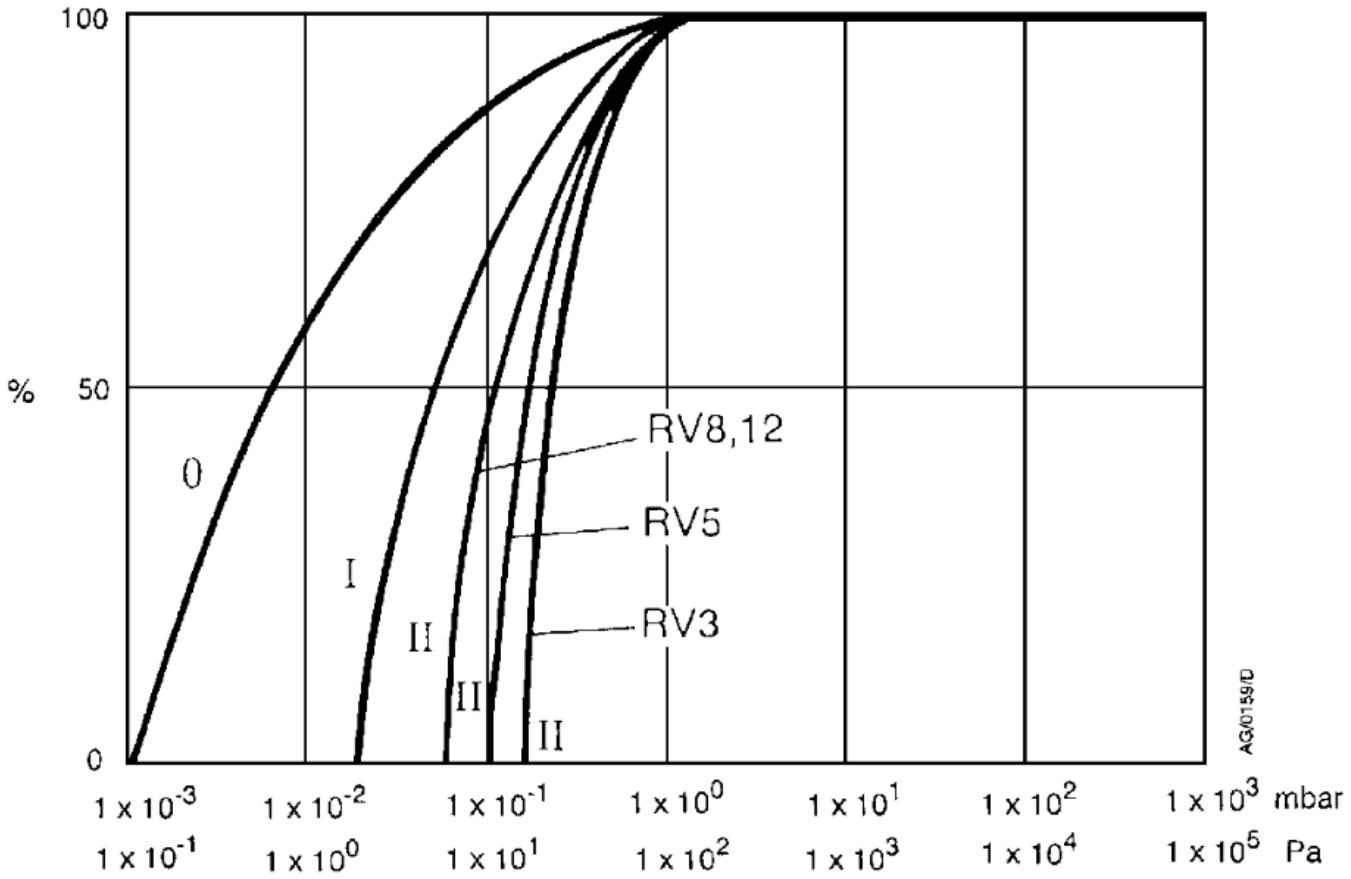

Figure .0.3: Characteristic of Edwards 12 RV12 vacuum pump [3]

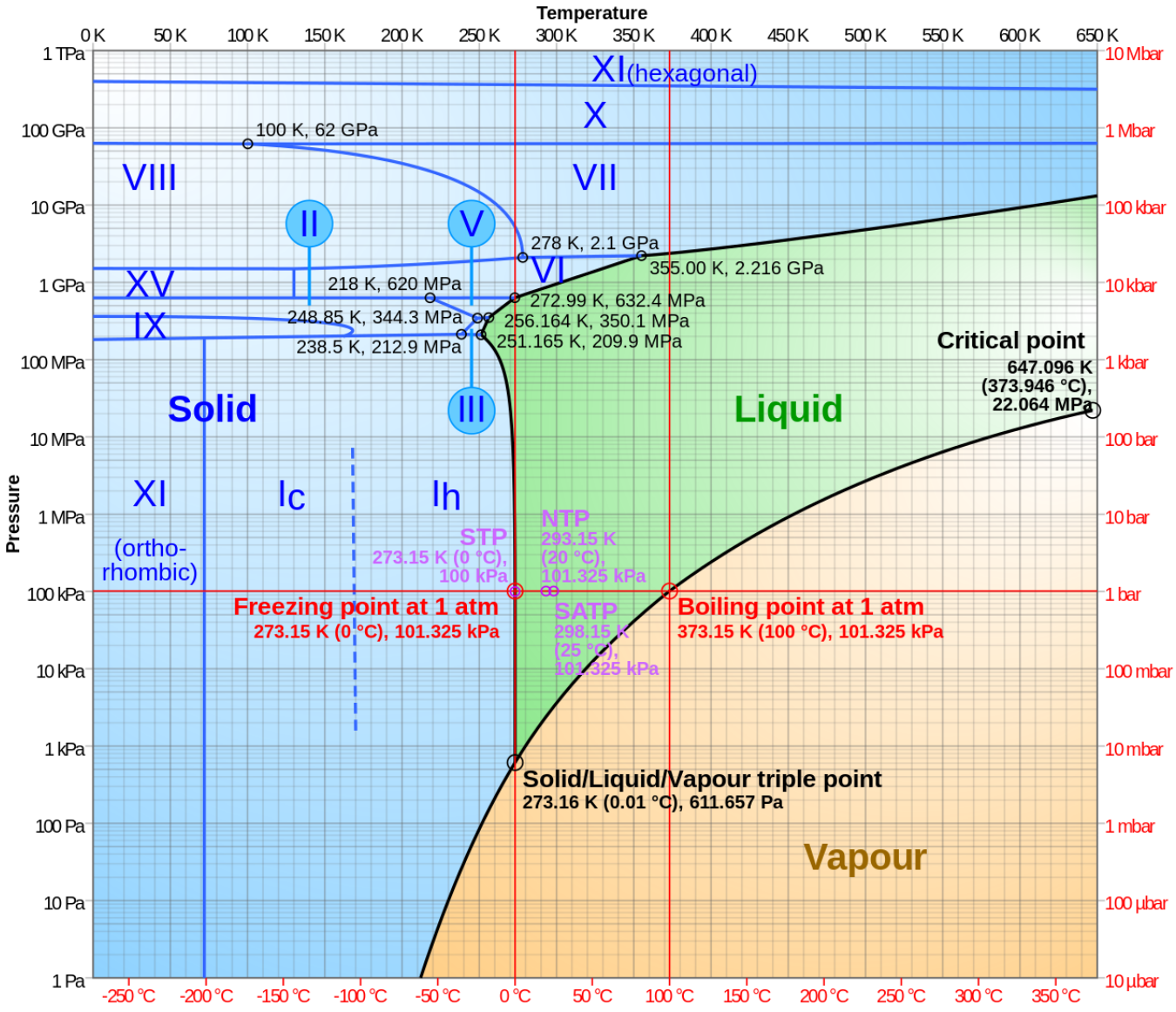

Figure .0.4: Water phase diagram [4]

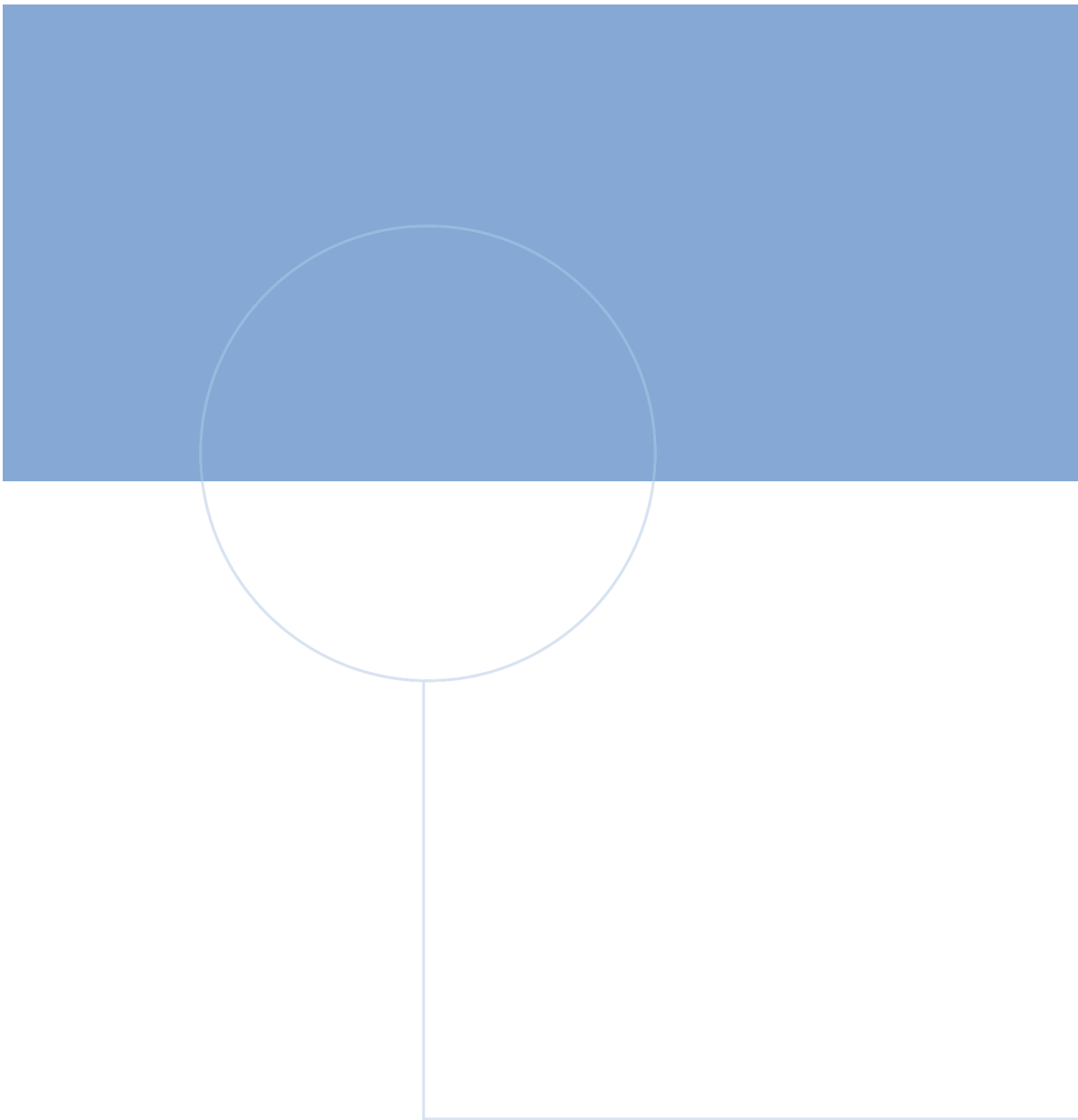

NTNU

Norwegian University of
Science and Technology